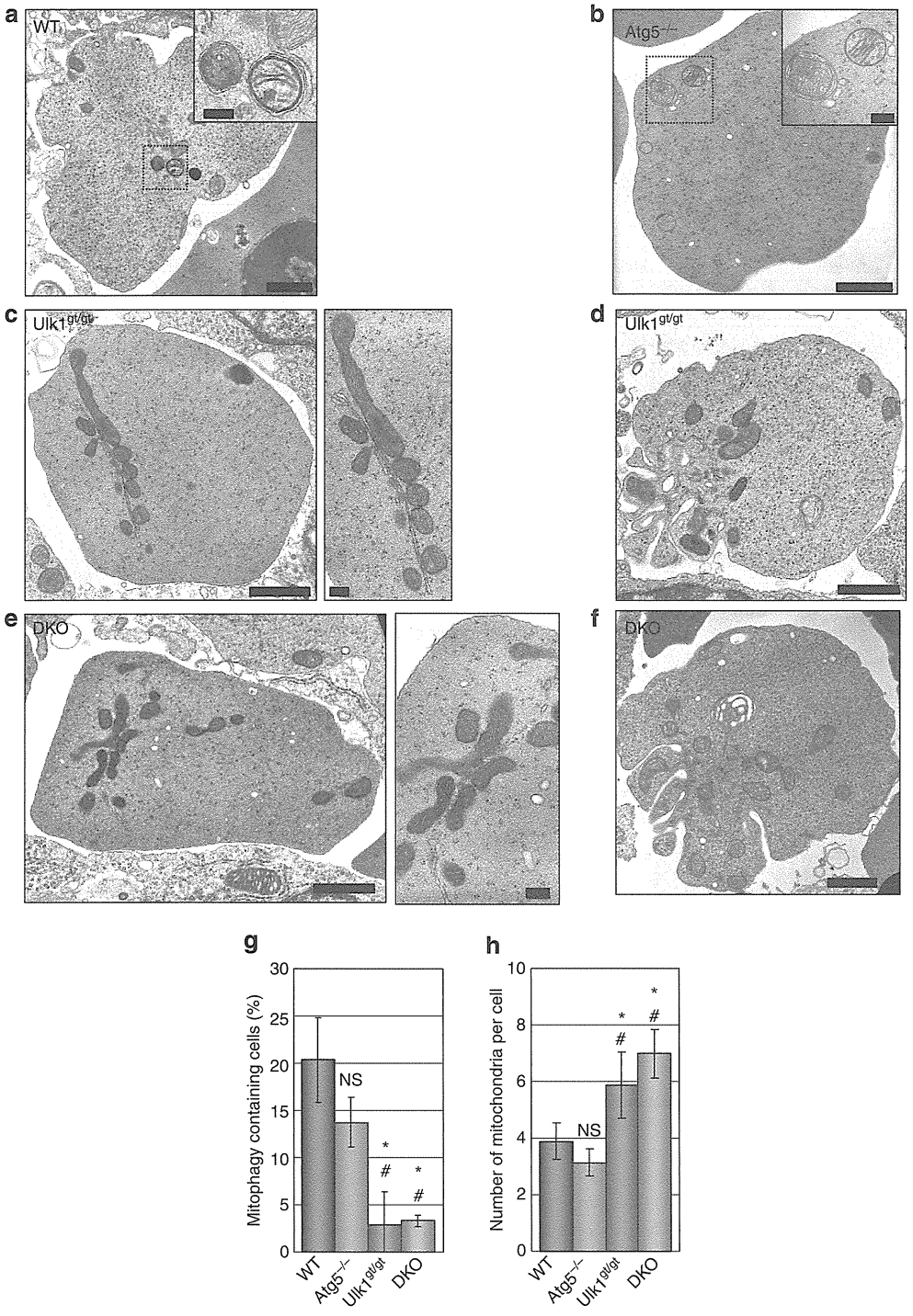

Figure 4 | Clearance of mitochondria by macroautophagy from reticulocytes of WT and Atg5$^{-/-}$ mice, but not Ulk1$^{gt/gt}$ or DKO mice. (**a**–**f**) Representative EM of WT (**a**), ATG5$^{-/-}$ (**b**), Ulk1$^{gt/gt}$ (**c**,**d**) and DKO (**e**,**f**) reticulocytes from embryonic liver (E14.5). (**a**,**b**) Mitophagy was detected in WT and ATG5$^{-/-}$ cells (scale bar, 1 μm). Insets indicate mitophagy (scale bar, 0.2 μm). (**c**,**e**) In Ulk1$^{gt/gt}$ and DKO cells, numerous mitochondria were in contact with membrane structures (scale bar, 1 μm). Enlarged images are shown on the right side (scale bar, 0.2 μm). (**d**,**f**) Some Ulk1$^{gt/gt}$ and DKO cells showed plasma membrane blebs containing mitochondria (scale bar, 1 μm). (**g**,**h**) Quantitative analysis of mitophagy calculated from EM photos in the embryonic liver at E18.5. Population of reticulocytes with mitophagy (**g**), and number of mitochondria per reticulocytes (**h**) were calculated ($n>35$ cells per mouse). The data are shown as mean ± s.d. ($n=3$). *$P<0.05$ versus value of WT (analysis of variance (ANOVA)); #$P<0.05$ versus value of Atg5$^{-/-}$ (ANOVA); 'NS' indicates not significant versus value of WT (ANOVA).

would not contribute to mitochondrial clearance from fetal definitive reticulocytes.

The WT and Atg5$^{-/-}$ reticulocytes expressed a high molecular weight Ulk1 isoform, compared with their erythroblasts (Fig. 5a). Ulk1 is regulated by posttranslational modifications such as phosphorylation[8,9] and acetylation[10]. Since the Ulk1 modification in reticulocytes was not changed by phosphatase treatment (Fig. 5c), Ulk1 acetylation, but not phosphorylation, seems to be crucial for mitochondrial clearance, although the possibility was not excluded that unidentified

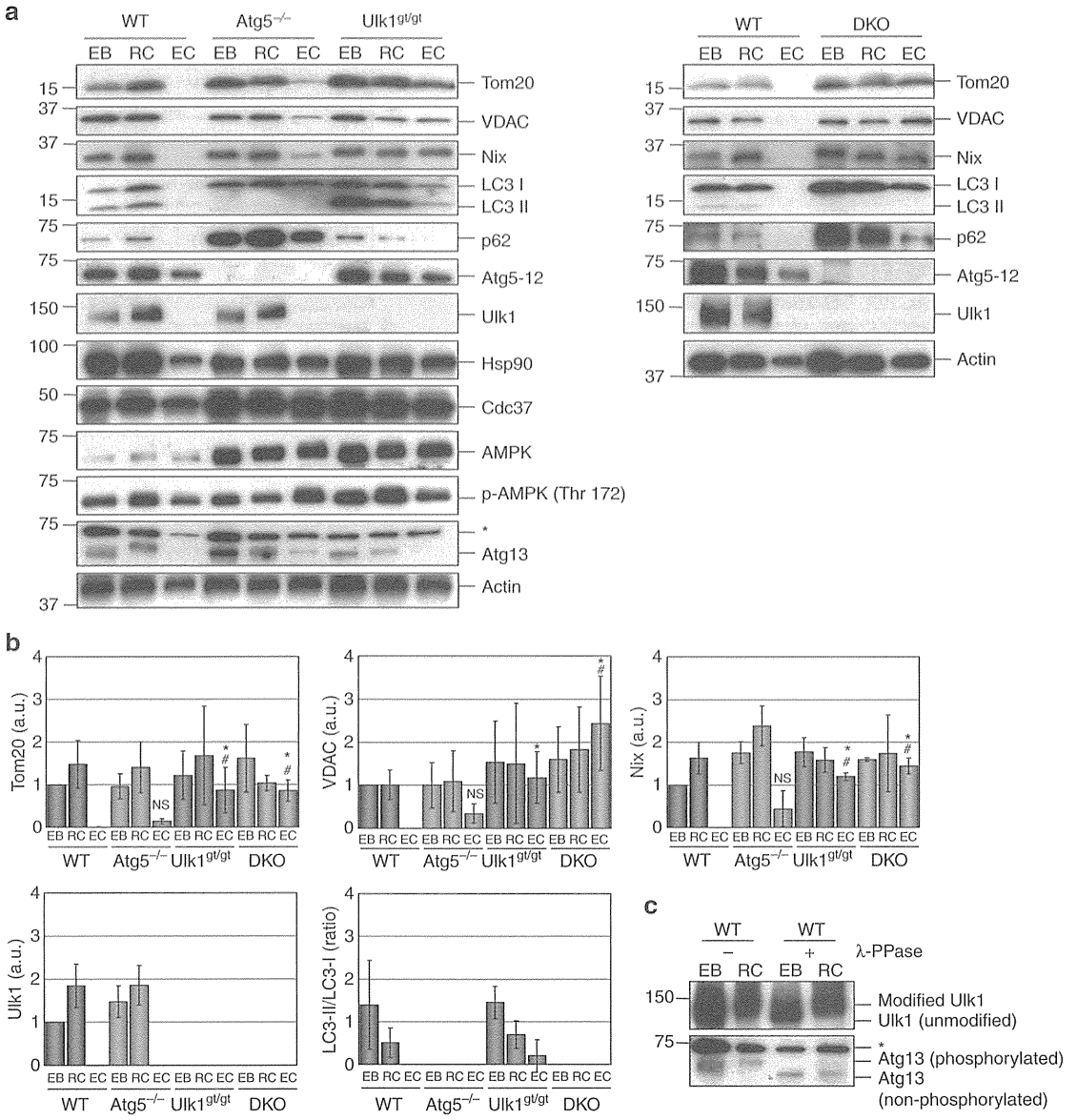

Figure 5 | Expression of autophagy-related proteins during erythrocyte differentiation. (**a**) Erythroblasts (EB; mitochondria^{high} Syto16^{high}), reticulocytes (RC; mitochondria^{high} Syto16^{low}) and EC (EC; Ter119^{+} PBC) were collected from the indicated embryos (E18.5), and the expression of each protein was examined by western blot. The asterisk indicates a nonspecific band. Uncropped images are shown in Supplementary Figs 11 and 12. (**b**) Semi-quantitative analysis of the expression level of each protein and the LC3-II/LC3-I ratio (mean ± s.d., $n=3$). $^{*}P<0.05$ versus value of WT EC (analysis of variance (ANOVA)); $^{\#}P<0.05$ versus value of Atg5$^{-/-}$ EC (ANOVA); 'NS' indicates not significant versus value of WT EC (ANOVA). (**c**) Modification of Ulk1 and Atg13 during erythrocyte maturation. Cell lysates were treated with λ-phosphatase (400 U) for 45 min at 30 °C, and band shift was examined by anti-Ulk1 and anti-Atg13 antibodies. Asterisk indicates non-specific band. Uncropped images are shown in Supplementary Fig. 12.

modification occurs in Ulk1. Although Hsp90, Cdc37 and AMPK were recently found responsible for Ulk1 activation[8,9], these proteins were slightly upregulated in WT reticulocytes, but not in Atg5$^{-/-}$ reticulocytes (Fig. 5a) despite the occurrence of mitophagy. In addition, a downstream effector of Ulk1 (Atg13) may be phosphorylated in WT reticulocytes (based on phosphatase reaction (Fig. 5c)), but not in Atg5$^{-/-}$ reticulocytes (Fig. 5a). These data support the existence of an unidentified Ulk1-mediated signalling pathway promoting cell differentiation in Atg5$^{-/-}$ reticulocytes.

Mitochondrial removal by alternative macroautophagy *in vitro*. The involvement of alternative macroautophagy in mitochondrial clearance during erythrocyte maturation was further confirmed using an *in vitro* erythrocyte differentiation system. Nascent erythroblasts were purified from the liver of E14.5 embryos and cultured in erythrocyte differentiation medium (see Methods). Three days after the induction of differentiation, >60% of the cells had lost their nuclei and become reticulocytes in every genotype (Fig. 6a,b). Thereafter, the enucleated cells (Syto16^{low} cells) lost their mitochondria in the cultures of WT cells, as shown by a gradual increase in the number of mitochondria^{low} Syto16^{low} cells (mature red blood cells) (Fig. 6c,d). Similar results were obtained with Atg5$^{-/-}$ erythroid cells. In contrast, the number of mitochondria^{low} Syto16^{low} cells did not increase in Ulk1$^{gt/gt}$ and DKO cells (Fig. 6c,d), indicating that Ulk1 is essential for mitochondrial clearance during *in vitro* differentiation, which is consistent with the *in vivo* findings. Wortmannin and 3-methyladenine are frequently used autophagy inhibitors known to inhibit both conventional and alternative

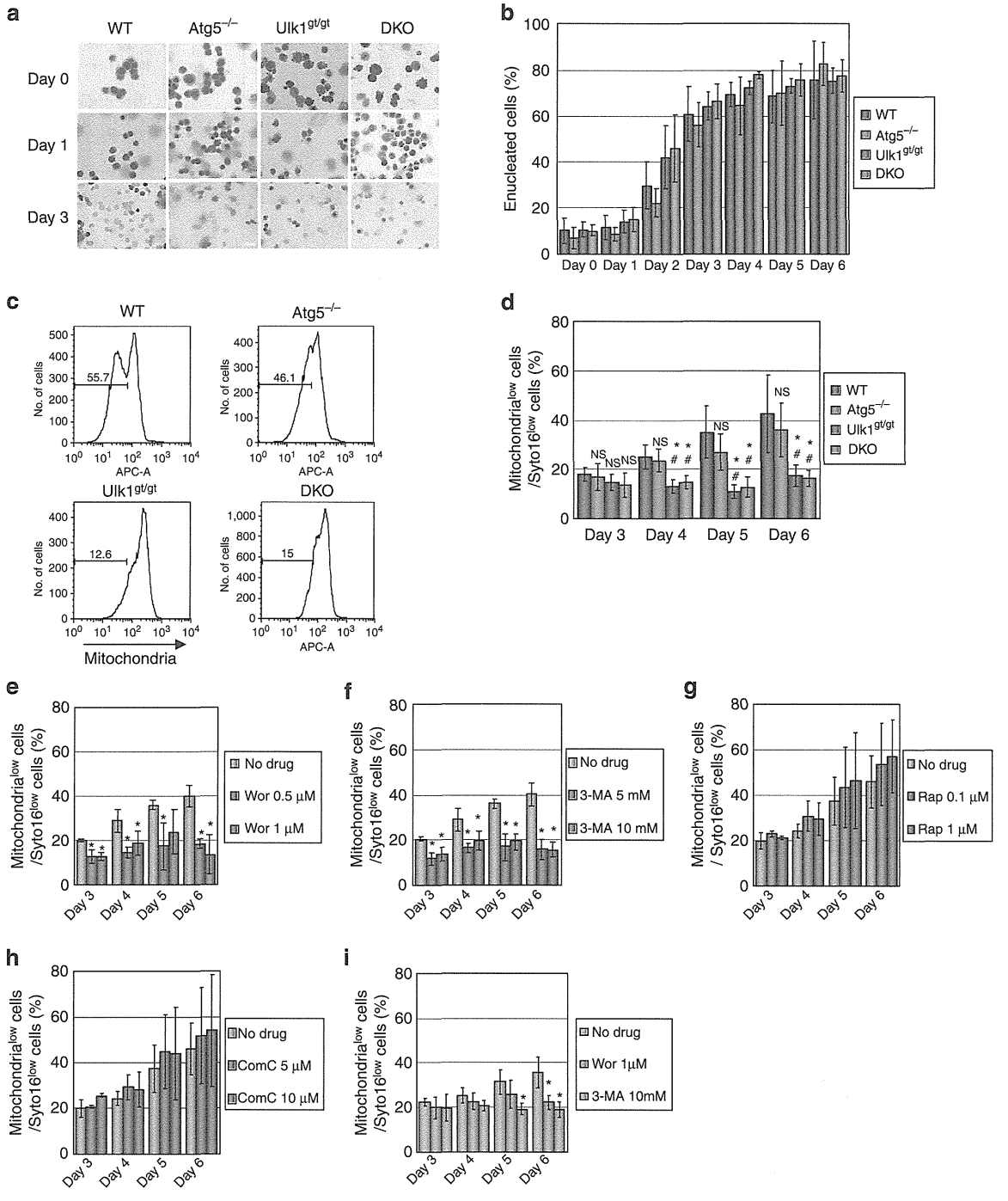

Figure 6 | Role of alternative macroautophagy in mitochondrial clearance during erythrocyte differentiation *in vitro*. (**a**) Morphology of cultured erythroid cells on day 0, 1 and 3 of differentiation. Erythroblasts were purified from embryonic liver (E14.5) and incubated for the indicated times in erythrocyte differentiation medium. The cells were stained with a Diff-quick kit. (**b**) Percentage of cells without nuclei (Syto16^{low} cells) on the indicated days of differentiation (mean ± s.d., $n=6$). Loss of nuclei occurred normally in all mice. (**c**,**d**) Percentage of Syto16^{low} cells without mitochondria. Differentiated cells were stained with Syto16 and Mitotracker Deep Red. Representative histograms of mitochondrial content in Syto16^{low} cells on day 6 are shown in (**c**). Numbers indicate the population of mitochondria^{low} cells. Representative dot plots are also available in Supplementary Fig. 13. (**d**) Percentage of Syto16^{low} cells lacking mitochondria determined by gating the mitochondria^{low} fraction as shown in (**c**) (mean ± s.d., $n=6$). $^{*}P<0.05$ versus value of WT (analysis of variance (ANOVA)); $^{\#}P<0.05$ versus value of Atg5$^{-/-}$ (ANOVA); 'NS' indicates not significant versus value of WT (ANOVA). (**e**–**h**) Impact of various drugs on mitochondrial clearance during *in vitro* differentiation. Differentiated cells from WT embryos were incubated with or without wortmannin (**e**), 3-methyladenine (3-MA) (**f**), rapamycin (**g**) or compound C (**h**) at the indicated concentrations and time periods. Percentage of mitochondria^{low} cells/Syto16^{low} cells was measured by flow cytometry (mean ± s.d., $n=3$). $^{*}P<0.05$ versus value of no drug (ANOVA). (**i**) Similar experiments were performed with cells from Atg5$^{-/-}$ embryos exposed to wortmannin or 3-MA (mean ± s.d., $n=3$). $^{*}P<0.05$ versus value of no drug (ANOVA).

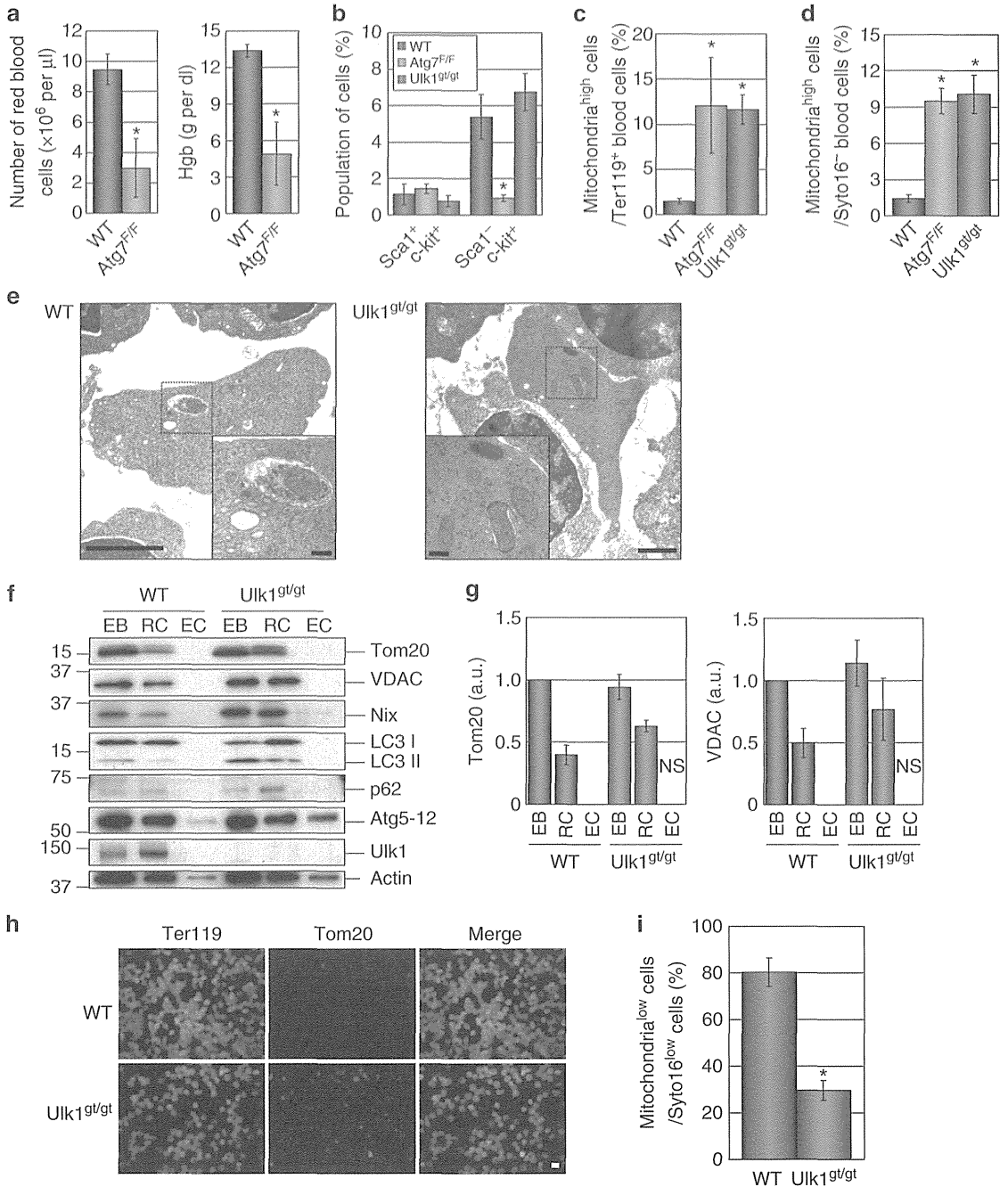

Figure 7 | Analysis of mitochondrial clearance during adult erythropoiesis. (**a**) Number of EC and haemoglobin content in the blood of the indicated mice (10–20 weeks old; mean ± s.d., $n=6$). *$P<0.05$ versus value of WT (Student's *t*-test). (**b**) Analysis of early erythrocyte development. Bone marrow cells were harvested from the indicated mice (10–20 weeks old) and stained with anti-cKit and anti-Sca1 antibodies. The population of each cell type was counted by FACS (mean ± s.d., $n=3$). *$P<0.05$ versus value of WT (analysis of variance (ANOVA)). (**c**) Percentage of mitochondria-containing Ter119$^+$ blood cells. Cells in peripheral blood from the indicated mice (10–20 weeks old) were stained with anti-Ter119 antibody together with Mitotracker Deep Red. The population of mitochondria^{high} cells among Ter119-positive cells was counted by FACS (mean ± s.d., $n=3$). *$P<0.05$ versus value of WT (ANOVA). (**d**) Percentage of mitochondria-containing Syto16^{low} blood cells. Cells in peripheral blood from the indicated mice (10–20 weeks old) were stained with Syto16 and Mitotracker Deep Red. The population of mitochondria^{high} cells among Syto16-negative cells was counted by FACS (mean ± s.d., $n=3$). *$P<0.05$ versus value of WT (ANOVA). (**e**) Representative electron micrographs of bone marrow reticulocytes in 10 week-old WT and Ulk1$^{gt/gt}$ mice (scale bar, 1 μm). Insets indicate mitophagy (scale bar, 0.2 μm). (**f**,**g**) Erythroblasts (EB; mitochondria^{high} Syto16^{high}), reticulocytes (RC; mitochondria^{high} Syto16^{low}) and EC (EC; Ter119$^+$ PBC) were collected from the indicated mice (10–20 weeks old), and the expression of each protein was examined by western blot. Uncropped images are shown in Supplementary Fig. 14. (**g**) Semi-quantitative analysis of the expression level of each protein (mean ± s.d., $n=3$). 'NS' indicates not significant versus value of WT EC (ANOVA). (**h**,**i**) The impact of Ulk1 on mitochondrial clearance during stress erythropoiesis. (**h**) Representative images of erythrocyte in PHZ-treated WT and Ulk1$^{gt/gt}$ mice (14 weeks old). Blood cells were stained with anti-Ter119 (erythroid cell marker) and anti-Tom20 (mitochondrial marker) antibodies and observed by fluorescence microscopy. Green and red indicate Ter119 and Tom20, respectively. Scale bar, 10 μm. (**i**) Percentage of mitochondria^{low} cells among Syto16^{low} cells. Erythroid cells were stained with Syto16 (DNA) and Mitotracker Deep Red (mean ± s.d., $n=3$). *$P<0.05$ versus value of WT (Student's *t*-test). Mitochondrial retention was observed in Ulk1$^{gt/gt}$ mice.

macroautophagy[6]. The addition of these inhibitors to the cultures of WT cells almost completely suppressed mitochondrial clearance from Syto16^{low} cells (Fig. 6e,f). These autophagy inhibitors also suppressed mitochondrial clearance in Atg5$^{-/-}$ cells (Fig. 6i), indicating this process was dependent on alternative macroautophagy. In contrast, rapamycin (conventional macroautophagy inducer) and compound C (AMPK inhibitor) did not have any effect (Fig. 6g,h). These data collectively indicate that alternative macroautophagy is responsible for mitochondrial clearance from embryonic reticulocytes.

Mitophagy in primitive and adult definitive reticulocytes. The contribution of Ulk1-dependent alternative macroautophagy was assessed in the other two waves of erythroid lineage: the primitive- and adult definitive lineages. The primitive wave emerges within the yolk sac blood islands[23]. The role of Ulk1 in mitochondrial clearance was examined in primitive erythrocyte by analysing whole blood in embryo at E11.5. Enucleation and mitochondrial clearance in Ulk1$^{gt/gt}$ erythroid cells were normally induced, as assessed by Syto16 and Mitotracker Deep Red staining, respectively (Supplementary Fig. 7). Therefore Ulk1 is not involved in the maturation of first primitive erythroid cells.

Adult definitive erythroid cells were investigated using Atg7$^{F/F}$Cre adult mice exhibiting abnormal mitochondrial clearance during erythrocyte maturation[18]. We hypothesized that adult and embryonic Atg7$^{F/F}$Cre mice express distinct mechanisms of mitochondrial clearance. To test this possibility, we compared peripheral blood cells (PBC) from WT, Ulk1$^{gt/gt}$ and Atg7$^{F/F}$Cre adult mice. The Atg7$^{F/F}$Cre mice exhibited the typical severe anaemia (Fig. 7a) as previously reported. This is likely due to a failure of early stage erythrocyte differentiation because the bone marrow Sca1^{-}c-Kit^{+} progenitors were severely downregulated (Fig. 7b), as previously reported[22]. Analysis of circulating EC indicated that the population of mitochondria-containing Ter119^{+} cells was higher in Atg7$^{F/F}$Cre mice and Ulk1$^{gt/gt}$ mice than in WT mice (Fig. 7c), but the population of mitochondria^{high} Ter119^{+} cells accounted for only 10% of all cells in both mice, which was considerably lower than those in the embryos. Similar results were obtained when the mitochondria-containing cells were counted among the Syto16^{low} cells (Fig. 7d). Furthermore, mitophagy was detected in bone marrow erythroid cells of Ulk1$^{gt/gt}$ mice (Fig. 7e). Based on western blot analysis, mitochondrial clearance was almost normal in the bone marrow erythroid cells of Ulk1$^{gt/gt}$ mice (Fig. 7f,g). These data indicate that the effect of Ulk1 and Atg7 on mitochondrial clearance from adult definitive reticulocytes was far less prominent than in fetal definitive reticulocytes.

Finally, we tested the contribution of Ulk1 to mitochondrial clearance during stress erythropoiesis. Acute anaemic stress triggers the rapid accumulation of new EC by a process distinct from steady-state erythropoiesis, and resembling the one of fetal definitive erythroid cells. Stress erythropoiesis was induced *in vivo* by injecting WT and Ulk1$^{gt/gt}$ mice with the haemolytic agent phenylhydrazine (PHZ)[24]. These mice showed significant and comparable reductions in the number of circulating EC, compared with untreated mice (Supplementary Fig. 8). Mitochondrial clearance was less efficient in PHZ-treated Ulk1$^{gt/gt}$ mice than in PHZ-treated WT mice (Fig. 7h,i), unlike steady-state erythropoiesis. These data suggest that Ulk1-dependent alternative macroautophagy is also involved in stress erythropoiesis.

Discussion

The present study demonstrated the contributions of alternative macroautophagy to mitochondrial clearance during the differentiation of EC. The main findings are as follows: First, mitochondrial clearance from reticulocytes occurs mainly by Ulk1-dependent Atg5-independent alternative macroautophagy in fetal definitive erythroid cells. Second, the impact of Ulk1 on mitochondrial clearance is markedly reduced in adult mice. Third, Atg7$^{F/F}$Cre mice exhibited severe anaemia; this anaemia was probably due to abnormal early differentiation as reported previously[25]. These findings support a new physiological role for Ulk1-dependent alternative macroautophagy during erythrocyte development, and the existence of Ulk1-independent processes in mature mammals. The role of Ulk1 in mitochondrial clearance from reticulocytes was previously described[8,11], but the molecular mechanisms have not been elucidated. Because Ulk1 was described as an initiator of conventional Atg5/Atg7-dependent macroautophagy, it is generally believed that mitochondria are digested by conventional macroautophagy. However, we recently discovered that mammalian cells conduct Atg5-independent macroautophagy largely regulated by Ulk1 (ref. 6). Therefore, we hypothesized that Ulk1-dependent Atg5-independent macroautophagy plays a role in mitochondrial clearance during erythrocyte differentiation, and found that mitophagy was detected in WT and Atg5$^{-/-}$ reticulocytes, but not in Ulk1$^{gt/gt}$ and DKO reticulocytes. We also demonstrated that mitochondria were retained in mature erythroid cells of Ulk1$^{gt/gt}$ and DKO embryos and the inhibition of alternative macroautophagy almost completely prevented mitochondrial clearance from Atg5$^{-/-}$ EC *in vitro*. In accordance, we concluded that the lack of Atg5 had less effect on mitophagy than the lack of Ulk1. These results indicate that Ulk1 is crucial for mitochondrial clearance via alternative macroautophagy.

What are the signalling pathways implicated in alternative Ulk1-mediated Atg5-independent macroautophagy? The contribution of conventional Ulk1 effectors (that is, Hsp90, Cdc37, AMPK and Atg13) is unlikely because we have shown that modifications of these proteins were not correlated with mitophagy in Atg5$^{-/-}$ reticulocytes (Fig. 5). In contrast, Nix expression levels correlated with mitophagy in all mouse genotypes. Nix was reported to have a function for the partial elimination of mitochondria via conventional macroautophagy[19–21], and also found crucial for LC3-independent mitophagy[22]. The latter machinery may be identical to alternative macroautophagy. Therefore, Nix seems to be involved in the mitophagy mediated by both conventional and alternative macroautophagy. Note that our current data only proposes the possible involvement of Nix, and future studies will be required to identify the molecular mechanisms of mitophagy including Nix dependency.

Mice with organ-specific Atg5 and Atg7 deficiency show various abnormalities, indicating that conventional macroautophagy is crucial for organ development and homeostasis[26,27]. Therefore, why does alternative macroautophagy, and not conventional macroautophagy, have an essential role in fetal definitive erythrocyte maturation? One possible explanation would be that alternative macroautophagy is only activated in Atg5-deficient cells as a compensation mechanism for conventional macroautophagy. However, this explanation is not supported by the poor colocalization of LC3 and Tom20 in WT reticulocytes (Supplementary Figs 3 and 6). Another possibility would be the lack of proteins or lipids required for conventional macroautophagy in embryonic reticulocytes. However, this is also unlikely because conventional macroautophagy was observed in WT and Ulk1$^{gt/gt}$ reticulocytes (Fig. 5; immunoblot of p62 and LC3). A more plausible explanation would be that conventional and alternative macroautophagy are supported by distinct machineries activated by different stimuli, and the alternative macroautophagy is the dominant force of mitochondrial

clearance during fetal definitive erythropoiesis. Further studies will be required to identify the stimuli and conditions specific for conventional and alternative macroautophagy.

The present study also showed the data about mitochondrial clearance from adult definitive erythroid cells. Although engulfment and digestion of mitochondria by autophagic vacuoles were clearly observed in EC of adult mice (Fig. 7e), Atg7 and Ulk1 did not have an important role in this process. The involvement of the Ulk1 homologue, Ulk2, was ruled out because it is not expressed by erythroid cells in adult mice (Supplementary Fig. 9). Therefore, Ulk1/Ulk2-independent Atg5/Atg7-independent macroautophagy may occur in adult EC.

In conclusion, this study demonstrates that mitochondrial clearance by Ulk1-dependent Atg5-independent alternative macroautophagy is essential for erythrocyte differentiation during fetal definitive erythrocytosis, but not in mature mammals. The specific activation during organ development suggests that this process is supported by signalling machinery distinct from that of conventional Atg5/Atg7-dependent macroautophagy. Elucidation of these signalling pathways may lead to the identification of genetic markers of congenital haematologic diseases.

Methods

Generation of Ulk1$^{gt/gt}$ mice. To generate *Ulk1* gene trap mice, the ES cell line targeting the *ulk1* gene was purchased from the Texas A&M Institute for Genomic Medicine (TIGM; College Station, TX, USA). The gene trap vector 48 (VICTR48) was inserted into intron 3 (Supplementary Fig. 1). The ES cell clones were microinjected into blastocysts to generate gene trap chimeras. The chimeric mice were screened for the presence of the β-geo gene trap cassette. Gene trap-positive chimeras were intercrossed with C57BL/6 mice for at least eight generations. The Atg5$^{-/-}$ and Atg7-flox mice were described in other studies[28,29]. The vav1-cre mice were purchased from the Jackson Laboratory (Bar Harbor, ME, USA). All animal experiments were approved by the Institutional Animal Care and Use Committee of the Tokyo Medical and Dental University. Mice were bred at the Laboratory for Recombinant Animals (Medical Research Institute, Tokyo Medical and Dental University, Tokyo, Japan).

Antibodies and chemicals. The following polyclonal antibodies were used for immunoblot and immunofluorescence assays: anti-Ulk1 (Sigma-Aldrich, #A7481; 1:1,000), anti-Atg5 (Sigma-Aldrich, #A0731; 1:1,000), anti-p62 (MBL, #PM045; 1:1,000), anti-Tom20 (Santa Cruz, #sc-11415; WB: 1:2,500, IF: 1:500), anti-Hsp90 (CST, #4877; 1:1,000), anti-VDAC (CST, #4866; 1:1,000), anti-AMPK (CST, #2532; 1:1,000) and anti-phospho-AMPK (CST, #2971; 1:1,000). The following monoclonal antibodies were also used: anti-Atg13 (MBL, #M183-3; 1:1,000), anti-Cdc37 (Santa Cruz, #sc-13129; 1:300), anti-LAMP2 (Abcam, #ab13524; 1:100), anti-Ter119 (BD Biosciences, #553670; 1:200), anti-NIX (CST, #12396; 1:1,000)), anti-LC3 (NanoTools, #0231; WB 1:1,000), anti-LC3 (Cosmobio, #CTB-LC3-2-1C; IF: 1:100), and anti-Actin (Millipore, #MAB1501; 1:2,500).

Flow cytometry was conducted with fluorescein isothiocyanate (FITC)-labelled anti-CD71 (BD Biosciences, #553266; 1:200), PE-labelled anti-Ter119 (BD Biosciences, #553673; 1:200), FITC-labelled anti-Sca1 (BD Biosciences, #557405; 1:200) and PE-labelled anti-cKit (BD Biosciences, #553355; 1:200) antibodies. The chemicals 3-methyladenine, rapamycin and compound C were obtained from Sigma-Aldrich, Santa Cruz and Calbiochem, respectively. Mitotracker Deep Red (#M22426), Syto-16 (#S7578) and DAPI (#P36935) were purchased from Molecular Probes. SCF (#250-03) and insulin-like growth factor-1 (#100-11) were obtained from PeproTech, whereas dexamethasone (#D2915), holo-Transferrin (#T1283) and PHZ (#P26252) were obtained from Sigma-Aldrich. Recombinant human erythropoietin (EPO; #HZ-1021) and recombinant human insulin (#O105) were obtained from HumanZyme and CSTI, respectively. The other chemicals were purchased from Nacalai Tesque (Tokyo, Japan).

Cell isolation. Ter119-positive erythroid lineage cells were isolated from mouse liver at embryonic day 18.5 (E18.5) using magnetic beads conjugated with anti-Ter119 antibody (BD IMag cell separation system). Erythroblasts (mitochondria^{high} Syto16^{high}) and reticulocytes (mitochondria^{high} Syto16^{low}) were isolated by cell sorting using a FACS Aria II (BD Biosciences). EC were collected from the peripheral blood using the IMag cell separation system.

Immunoblot analysis. Cell samples were homogenized in SDS sample buffer and loaded on SDS-polyacrylamide gels. The protein bands were transferred to polyvinylidene difluoride membranes (Millipore). The membranes were blocked with 3% skim milk in TBS containing 0.1% Tween-20 (TBS-T), and then incubated with the primary antibody overnight at 4 °C. After washes in TBS-T, the membranes were incubated with the horseradish peroxidase-labelled secondary antibody and visualized with Chemi-Lumi One Super reagent. Protein band density was semi-quantified using ImageJ software. Protein dephosphorylation of Ulk1 and Atg13 was conducted by incubating cell lysates with 400 U λ-phosphatase (45 min; 30 °C) and band shift was examined by western blot analysis. All experiments were conducted at least in triplicates. We supplied several uncropped scans of the western blots in Supplementary Figures.

Immunofluorescence analysis. Cells were fixed in 4% paraformaldehyde, pelleted on slides by cytospin3 (Shandon), and stained with primary antibodies for 1 h at room temperature. After washes, the cells were stained with secondary antibodies, mounted in ProLong Gold antifade reagent with DAPI, and examined by confocal microscopy (LSM510 Zeiss).

Electron microscopy. Cells were fixed with 1.5% paraformaldehyde/3% glutaraldehyde in 0.1 M phosphate buffer (pH 7.3), followed by 1% OsO_4. After dehydration, the fixed cells were embedded in Epon812. Thin sections were cut and stained with uranyl acetate lead citrate for observation under a JEM-1010 electron microscope (JEOL Co. Ltd.) at 80 k.

Analysis of erythroid differentiation. Erythroid cells were obtained from the liver and peripheral blood of embryonic E18.5 mice. Hepatic erythroid cells were isolated from liver tissue using a 70-μm cell strainer. Erythroid cells were also obtained from the bone marrow and peripheral blood of adult mice. For three-colour analysis of erythrocyte differentiation and mitochondria, the cells were incubated with PE-conjugated anti-Ter119, FITC-conjugated anti-CD71 antibody, and Mitotracker Deep Red (30 min; 4 °C). For two-colour analysis of nuclei and mitochondria, the cells were incubated with Syto-16 and Mitotracker Deep Red (30 min; 4 °C). For the analysis of early erythrocyte differentiation, bone marrow cells were incubated with PE-conjugated anti-cKit and FITC-conjugated anti-Sca1 antibody (30 min; 4 °C). Stained cells were washed with PBS and analysed by flow cytometry with a FACS CantII (BD Biosciences). Data analysis was performed with BD FACSDiva and Flowjo software.

***In vitro* erythroid differentiation.** Erythroblasts were purified from embryonic mouse liver (E14.5), and then suspended at 1×10^6 cells ml^{-1} in a 24-well gelatin-coated tissue culture dish containing StemPro34 plus Nutrient Supplement (Invitrogen) with 2 units ml^{-1} of human EPO, 100 ng ml^{-1} of SCF, 10^{-6} M dexamethasone, 40 ng ml^{-1} of insulin-like growth factor-1 and penicillin/streptomycin. After 1 or 3 days of culture, the nonadherent cells were collected, filtered through a 70-μm cell strainer and transferred to a fresh gelatin-coated dish for the induction of differentiation as follows. In brief, erythroblasts were washed with PB2 buffer (0.1% glucose and 0.3% bovine serum albumin in PBS), and suspended in Iscove's modified Dulbecco's medium containing 15% fetal bovine serum, 1% detoxified bovine serum albumin, 200 μg ml^{-1} of holo-Transferrin, 10 μg ml^{-1} of recombinant human insulin, 2 mM L-glutamine, 10^{-4} M β-mercaptoethanol and 2 units ml^{-1} of EPO. The cultures were examined after staining with a Diff-quick staining kit (Sysmex). Various agents were added on day 2 to assess their effects on cell differentiation. Mitochondrial clearance was examined by flow cytometry after staining with Syto-16 and Mitotracker Deep Red.

Stress hematopoiesis. Mice were injected subcutaneously with PHZ[24] (50 mg kg^{-1} in sterile saline). After 7 days, they were killed and blood was collected from the caudal vena cava.

Isolation of primitive erythrocyte. After removal of the placenta, embryos were transferred to dishes containing heparinized PBS. Blood cells were collected by aspiration as they bled.

Haematology tests. Peripheral blood samples were harvested in heparinized tubes, and analysed with a blood cell counter (ERMA Inc.) using the programme for mice.

Statistical analysis. Results are expressed as the mean ± s.d. Statistical evaluation was performed using Prism (GraphPad) software. Comparisons of two data sets were performed using unpaired two-tailed Student's *t*-test. All other comparisons of multiple data sets were performed using one-way analysis of variance followed by Tukey's *post hoc* test. Statistical significance was established for *P*-values of <0.05.

References

1. Xie, Z. & Klionsky, D. J. Autophagosome formation: core machinery and adaptations. *Nat. Cell Biol.* **9,** 1102–1109 (2007).
2. Mizushima, N., Levine, B., Cuervo, A. M. & Klionsky, D. J. Autophagy fights disease through cellular self-digestion. *Nature* **451,** 1069–1075 (2008).

3. Nakatogawa, H., Suzuki, K., Kamada, Y. & Ohsumi, Y. Dynamics and diversity in autophagy mechanisms: lessons from yeast. *Nat. Rev. Mol. Cell Biol.* **10,** 458–467 (2009).
4. Mizushima, N., Yoshimori, T. & Ohsumi, Y. The role of Atg proteins in autophagosome formation. *Annu. Rev. Cell Dev. Biol.* **27,** 107–132 (2011).
5. Axe, E. L. *et al.* Autophagosome formation from membrane compartments enriched in phosphatidylinositol 3-phosphate and dynamically connected to the endoplasmic reticulum. *J. Cell Biol.* **182,** 685–701 (2008).
6. Nishida, Y. *et al.* Discovery of Atg5/Atg7-independent alternative macroautophagy. *Nature* **461,** 654–658 (2009).
7. Hosokawa, N. *et al.* Atg101, a novel mammalian autophagy protein interacting with Atg13. *Autophagy* **7,** 973–979 (2009).
8. Joo, J. H. *et al.* Hsp90-Cdc37 chaperone complex regulates Ulk1- and Atg13-mediated mitophagy. *Mol. Cell* **43,** 572–585 (2011).
9. Egan, D. F. *et al.* Phosphorylation of ULK1 (hATG1) by AMP-activated protein kinase connects energy sensing to mitophagy. *Science* **331,** 456–461 (2011).
10. Lin, S. Y. *et al.* GSK3-TIP60-ULK1 signaling pathway links growth factor deprivation to autophagy. *Science* **336,** 477–481 (2012).
11. Kundu, M. *et al.* Ulk1 plays a critical role in the autophagic clearance of mitochondria and ribosomes during reticulocyte maturation. *Blood* **112,** 1493–1502 (2008).
12. Komatsu, M. & Ichimura, Y. Selective autophagy regulates various cellular functions. *Genes Cells* **15,** 923–933 (2010).
13. Ding, W. X. & Yin, X. M. Mitophagy: mechanisms, pathophysiological roles, and analysis. *Biol. Chem.* **393,** 547–564 (2012).
14. Kent, G., Minick, O. T., Volini, F. I. & Orfei, E. Autophagic vacuoles in human red cells. *Am. J. Pathol.* **48,** 831–857 (1966).
15. Heynen, M. J., Tricot, G. & Verwilghen, R. L. Autophagy of mitochondria in rat bone marrow erythroid cells. Relation to nuclear extrusion. *Cell Tissue Res.* **239,** 235–239 (1985).
16. Matsui, M., Yamamoto, A., Kuma, A., Ohsumi, Y. & Mizushima, N. Organelle degradation during the lens and erythroid differentiation is independent of autophagy. *Biochem. Biophys. Res. Commun.* **339,** 485–489 (2006).
17. Zhang, J. *et al.* Mitochondrial clearance is regulated by Atg7-dependent and -independent mechanisms during reticulocyte maturation. *Blood* **114,** 157–164 (2009).
18. Mortensen, M. *et al.* Loss of autophagy in erythroid cells leads to defective removal of mitochondria and severe anemia *in vivo*. *Proc. Natl Acad. Sci. USA* **107,** 832–837 (2010).
19. Schweers, R. L. *et al.* NIX is required for programmed mitochondrial clearance during reticulocyte maturation. *Proc. Natl Acad. Sci. USA* **104,** 19500–19505 (2007).
20. Sandoval, H. *et al.* Essential role for Nix in autophagic maturation of erythroid cells. *Nature* **454,** 232–235 (2008).
21. Novak, I. *et al.* Nix is a selective autophagy receptor for mitochondrial clearance. *EMBO Rep.* **11,** 45–51 (2010).
22. Zhang, J. *et al.* A short linear motif in BNIP3L (NIX) mediates mitochondrial clearance in reticulocytes. *Autophagy* **8,** 1325–1332 (2012).
23. Huber, T. L., Kouskoff, V., Fehling, H. J., Palis, J. & Keller, G. Haemangioblast commitment is initiated in the primitive streak of the mouse embryo. *Nature* **432,** 625–630 (2004).
24. Ulyanova, T., Jiang, Y. i., Padilla, S., Nakamoto, B. & Papayannopoulou, T. Combinatorial and distinct roles of α5 and α4 integrins in stress erythropoiesis in mice. *Blood* **117,** 975–985 (2011).
25. Mortensen, M. *et al.* The autophagy protein Atg7 is essential for hematopoietic stem cell maintenance. *J. Exp. Med.* **208,** 455–467 (2011).
26. Mizushima, N. & Komatsu, M. Autophagy: renovation of cells and tissues. *Cell* **147,** 728–741 (2011).
27. Choi, A. M., Ryter, S. W. & Levine, B. Autophagy in human health and disease. *New Engl. J. Med.* **368,** 651–662 (2013).
28. Kuma, A. *et al.* The role of autophagy during the early neonatal starvation period. *Nature* **432,** 1032–1036 (2004).
29. Komatsu, M. *et al.* Impairment of starvation-induced and constitutive autophagy in Atg7-deficient mice. *J. Cell Biol.* **169,** 425–434 (2005).

Acknowledgements

We are grateful to Dr N. Mizushima (University of Tokyo) for kindly providing $Atg5^{-/-}$ mice. We are also grateful to Drs. M. Komatsu and K. Tanaka (Rinshoken) for kindly providing Atg7-flox mice. This work was supported in part by the Grant-in-Aid for Scientific Research on Innovative Areas, Grant-in-Aid for Scientific Research (S), Grant-in-Aid for challenging Exploratory Research, Grant-in-Aid for Young Scientists (A) from the MEXT of Japan and a grant for the Scientific Technique Research Promotion Programme for Agriculture, Forestry, Fisheries and Food Industry. This study was also supported by grants from the following sources: The Secom Science and Technology Foundation, The Takeda Science Foundation, The Uehara Memorial Foundation, The Sumitomo Foundation and The SENSHIN Medical Research Foundation.

Author contributions

S.H. designed the research and performed biological analyses, Y.N. and H.Y. performed biological analyses, S.A. performed EM analyses, E.I. advised data interpretation, and S.S. designed the research and wrote the manuscript. All authors edited the manuscript.

Additional information

Supplementary Information accompanies this paper at http://www.nature.com/naturecommunications

Competing financial interests: The authors declare no competing financial interests.

Reprints and permission information is available online at http://npg.nature.com/reprintsandpermissions/

How to cite this article: Honda, S. *et al.* Ulk1-mediated Atg5-independent macroautophagy mediates elimination of mitochondria from embryonic reticulocytes. *Nat. Commun.* 5:4004 doi: 10.1038/ncomms5004 (2014).

OPEN ACCESS
CellPress

Cell Reports
Report

XIAP Restricts TNF- and RIP3-Dependent Cell Death and Inflammasome Activation

Monica Yabal,[1] Nicole Müller,[1] Heiko Adler,[2] Nathalie Knies,[3] Christina J. Groß,[3] Rune Busk Damgaard,[4,10] Hirokazu Kanegane,[5] Marc Ringelhan,[6] Thomas Kaufmann,[7] Mathias Heikenwälder,[6] Andreas Strasser,[8,9] Olaf Groß,[3] Jürgen Ruland,[3] Christian Peschel,[1] Mads Gyrd-Hansen,[4,10] and Philipp J. Jost[1,*]

[1]III. Medizinische Klink, Klinikum rechts der Isar, Technische Universität München, 81675 München, Germany
[2]Research Unit Gene Vectors, Helmholtz Zentrum München-German Research Center for Environmental Health, GmbH, 85764 Oberschleissheim, Germany
[3]Institut für Klinische Chemie und Pathobiochemie, Klinikum rechts der Isar, Technische Universität München, 81675 München, Germany
[4]Novo Nordisk Foundation Center for Protein Research, Faculty of Health and Medical Sciences, University of Copenhagen, 2200 Copenhagen, Denmark
[5]Department of Pediatrics, Graduate School of Medicine and Pharmaceutical Sciences, University of Toyama, 2630 Sugitani, Toyama 930-0194, Japan
[6]Institute of Virology, Technische Universität München and Helmholtz Zentrum München, 81675 München, Germany
[7]Institute of Pharmacology, University of Bern, 3010 Bern, Switzerland
[8]The Walter and Eliza Hall Institute of Medical Research, Parkville,VIC 3052, Australia
[9]Department of Medical Biology, University of Melbourne, Melbourne, VIC 3052, Australia
[10]Present address: Ludwig Cancer Research, Nuffield Department of Clinical Medicine, University of Oxford, Oxford OX3 7DQ, UK
*Correspondence: philipp.jost@lrz.tum.de
http://dx.doi.org/10.1016/j.celrep.2014.05.008

SUMMARY

X-linked inhibitor of apoptosis protein (XIAP) has been identified as a potent regulator of innate immune responses, and loss-of-function mutations in XIAP cause the development of the X-linked lymphoproliferative syndrome type 2 (XLP-2) in humans. Using gene-targeted mice, we show that loss of XIAP or deletion of its RING domain lead to excessive cell death and IL-1β secretion from dendritic cells triggered by diverse Toll-like receptor stimuli. Aberrant IL-1β secretion is TNF dependent and requires RIP3 but is independent of cIAP1/cIAP2. The observed cell death also requires TNF and RIP3 but proceeds independently of caspase-1/caspase-11 or caspase-8 function. Loss of XIAP results in aberrantly elevated ubiquitylation of RIP1 outside of TNFR complex I. Virally infected Xiap$^{-/-}$ mice present with symptoms reminiscent of XLP-2. Our data show that XIAP controls RIP3-dependent cell death and IL-1β secretion in response to TNF, which might contribute to hyperinflammation in patients with XLP-2.

INTRODUCTION

X-linked inhibitor of apoptosis protein (XIAP) is an antiapoptotic protein that inhibits induction of cell death in response to intrinsic as well as extrinsic apoptotic stimuli (Gyrd-Hansen and Meier, 2010; Jost et al., 2009). Inhibition of apoptosis by XIAP is mediated by inhibiting caspase-3 and caspase-7 via its N-terminal baculoviral IAP repeat (BIR) domains (Deveraux et al., 1997). The first characterization of *Xiap*$^{-/-}$ mice showed no obvious phenotype (Olayioye et al., 2005), whereas recent studies have demonstrated a reduced capacity of *Xiap*$^{-/-}$ mice to clear certain infectious pathogens (Bauler et al., 2008; Prakash et al., 2010). In addition, the RING domain and the BIR2 domain of XIAP have been implicated in nuclear factor-κB (NF-κB) and mitogen-activated protein kinase (MAPK) signaling in response to activation of nucleotide-binding oligomerization domain 1 (NOD1) and NOD2 (Damgaard et al., 2012, 2013).

To date, XIAP has not been implicated in tumor necrosis factor (TNF)/TNF receptor (TNFR) signaling despite a well-defined role for its close IAP family members, cellular inhibitor of apoptosis proteins 1 and 2 (cIAP1/cIAP2), in this pathway (Gyrd-Hansen and Meier, 2010). cIAP1/cIAP2-dependent K63 ubiquitylation of receptor-interacting protein 1 (RIP1) after TNF stimulation provides a prosurvival signaling platform allowing for the induction of NF-κB and MAPK signaling (Bertrand et al., 2008). Loss of cIAP1/cIAP2 or deubiquitylation of RIP1 coincides with the formation of secondary TNFR signaling complexes (TNF-RSCs) that trigger cell death either through caspase-8-mediated apoptosis or through RIP3- and MLKL-dependent necroptosis (Murphy et al., 2013; O'Donnell et al., 2011; Vince et al., 2007).

There are indications that elevated necroptosis contributes to inflammation and tissue damage, at least in part, mediated by interleukin-1β (IL-1β) (Günther et al., 2011; Kang et al., 2013). IL-1β is an evolutionarily conserved cytokine that potently mediates innate and adaptive immune responses, and its deregulation causes several autoinflammatory diseases (Lamkanfi and Dixit, 2012). IL-1β is translated as an inactive proform and requires processing into bioactive IL-1β by the inflammasome (Martinon et al., 2002).

Mutations within *BIRC4* (XIAP) have been identified as the genetic cause of the X-linked lymphoproliferative syndrome type 2 (XLP-2). The mutations mostly affect the C-terminal RING domain or result in complete loss of protein expression (Damgaard et al., 2013; Marsh et al., 2010; Pachlopnik Schmid et al., 2011). Clinical symptoms are mostly attributed to the aberrant activation of macrophages and dendritic cells (DCs) and the accumulation of activated T lymphocytes often in response to viral infection (Marsh et al., 2010). This hyperactivation of immune cells results in elevated systemic levels of proinflammatory cytokines, such as IL-1β, interferon-γ (IFNγ), TNF, IL-6, and IL-18 (Marsh et al., 2010; Rigaud et al., 2006; Wada et al., 2014).

We demonstrate here an unexpected function of XIAP in curtailing excessive TNF-induced inflammasome activation. This function was independent of cIAP1/cIAP2 and restricted IL-1β production in a RIP3-dependent manner. Viral infection of *Xiap*$^{-/-}$ mice resulted in a hyperinflammatory phenotype similar to that observed in patients with XLP-2, indicating that exaggerated IL-1β secretion might contribute to XLP-2 pathogenesis.

RESULTS

TLR Activation Induces Exaggerated IL-1β Secretion in *Xiap*$^{-/-}$ and *Xiap*$^{\Delta RING}$ Dendritic Cells

XLP-2 pathology in patients is mostly ascribed to a severe hyperinflammation in response to microbial infections. We therefore hypothesized that microbial ligands trigger deregulated immune responses in *Xiap*$^{-/-}$ mice. To study cytokine responses, we differentiated dendritic cslls (DCs) from bone marrow progenitors (BMDCs) of mice lacking XIAP or expressing a knockin allele of a RING-deleted version of XIAP termed *Xiap*$^{\Delta RING}$ (*Xiap* $^{\Delta RING/\Delta RING}$) (Olayioye et al., 2005; Schile et al., 2008) (Figure S1A). After treatment with ligands for Toll-like receptor 3 (TLR3), TLR4, and TLR9, we observed a significant increase of IL-1β secretion from *Xiap*$^{-/-}$ and *Xiap*$^{\Delta RING}$ BMDCs compared to wild-type (WT) BMDCs. Whereas TNF secretion from *Xiap*$^{-/-}$ and *Xiap*$^{\Delta RING}$ cells was comparable to WT, the exaggerated IL-1β secretion correlated with increased cell death (Figure 1A). A similar phenotype was also observed in bone marrow-derived macrophages (BMDMs) (Figure S1B). IL-1β secretion and cell death, measured by a decrease of intracellular ATP levels or lactate dehydrogenase (LDH) release, occurred between 4 and 8 hr of lipopolysaccharide (LPS) exposure only in *Xiap*$^{-/-}$ BMDCs (Figure 1B). However, NF-κB and MAPK signaling and subsequent gene induction were largely identical in both genotypes (*Xiap*$^{-/-}$ and WT) in response to LPS, despite a minor elevation of phosphorylated p38 in *Xiap*$^{-/-}$ cells (Figures 1C and S1C). The elevated secretion of IL-1β in *Xiap*$^{-/-}$ BMDCs in response to LPS was remarkable because conventional inflammasome activation requires a priming and an activating signal, such as ATP, for inflammasome formation (Gross et al., 2012; Martinon et al., 2002). The hypersecretion of IL-1β correlated with the formation of conventional inflammasome complexes as shown by accumulation of NOD-like receptor family pyrin domain-containing 3 (NLRP3), Apoptosis-associated Speck-like protein containing a CARD (ASC), and caspase-1 within the NP-40-insoluble fraction only in *Xiap*$^{-/-}$ cells, but not in WT cells treated with LPS only (Figure 1D). WT BMDCs recruited ASC and caspase-1 into the NP-40 fraction only after treatment with LPS plus ATP (Figure 1D). We also observed recruitment of caspase-8 into the NP-40 fraction in *Xiap*$^{-/-}$ cells but not in WT cells after LPS treatment (Figure 1D). Immunofluorescence microscopy further confirmed ASC/caspase-1 speck formation in *Xiap*$^{-/-}$ BMDCs treated with LPS only (Figure 1E), whereas speck formation in WT cells required the addition of ATP or nigericin (Gross et al., 2012) (Figures 1D and 1E).

Of note, conventional inflammasome activation in response to ATP (Figure S1D) or nigericin (Figure 1E), and inflammasome inhibition by blocking potassium efflux or by caspase inhibition (Figure S1E), was identical in WT and *Xiap*$^{-/-}$ BMDCs. Together, this demonstrated that the priming signal alone induced substantial inflammasome formation and IL-1β secretion in *Xiap*$^{-/-}$ BMDCs, but not in WT BMDCs.

Because necrotic cell death can activate the inflammasome (Lamkanfi and Dixit, 2012), we examined the connection between IL-1β secretion and cell death. To characterize the contribution of damage-associated molecular pattern molecules (DAMPs) released from dying cells to the IL-1β secretion observed, we costimulated BMDCs with LPS plus lysates from dead cells generated by repeated freeze-thaw cycles. This treatment failed to further enhance IL-1β secretion after LPS (Figure S1F). In addition, we cocultured WT and *Xiap*$^{-/-}$ BMDCs prior to LPS stimulation. Supporting a DAMP-independent cause of inflammasome activation, we observed caspase-1 specks only in *Xiap*$^{-/-}$ cells, whereas directly adjacent WT cells did not contain specks (Figure S1G). Our data argue that cell-intrinsic signaling aberrations in *Xiap*$^{-/-}$ and *Xiap*$^{\Delta RING}$ BMDCs resulted in increased inflammasome formation.

Similar to the systemic cytokinemia observed in patients with XLP-2, we hypothesized that activation of the innate immune system might drive an exaggerated inflammatory response. This was confirmed in a murine model of acute peritonitis elicited by intraperitoneal (i.p.) injection of LPS or the adjuvant alum, which both resulted in increased IL-1β levels in the peritoneal fluid of *Xiap*$^{-/-}$ mice when compared to WT (Figures 1F and 1G). These data show that TLR stimulation of DCs caused elevated inflammasome formation and IL-1β secretion in vitro and in vivo when XIAP was missing.

IL-1β Secretion in Response to LPS in *Xiap*$^{-/-}$ BMDCs Is Mediated by TNF Signaling

We next examined what factors control the IL-1β secretion in *Xiap*$^{-/-}$ cells. IL-1β secretion was reduced by caspase-1 inhibitor treatment (YVAD), whereas an IL-1β receptor antagonist (IL-1RA; anakinra) did not substantially reduce IL-1β levels in *Xiap*$^{-/-}$ BMDCs, although some reduction was seen in *Xiap*$^{\Delta RING}$ cells (Figure S2A). This argues against a prominent role for autocrine or paracrine IL-1 receptor signaling. In contrast, anti-TNF-α (Enbrel) potently inhibited IL-1β secretion, reduced cell death, and blocked processing of caspase-8 in *Xiap*$^{-/-}$ and *Xiap*$^{\Delta RING}$ BMDCs (Figures S2A and S2B).

In line with a possible role of XIAP in regulating signaling events downstream of TNF/TNFR, we observed elevated IL-1β secretion and cell death in *Xiap*$^{-/-}$ and *Xiap*$^{\Delta RING}$ BMDCs in response to recombinant TNF (Figure 2A). This was interesting because XIAP has not been directly implicated in TNF/TNFR signal

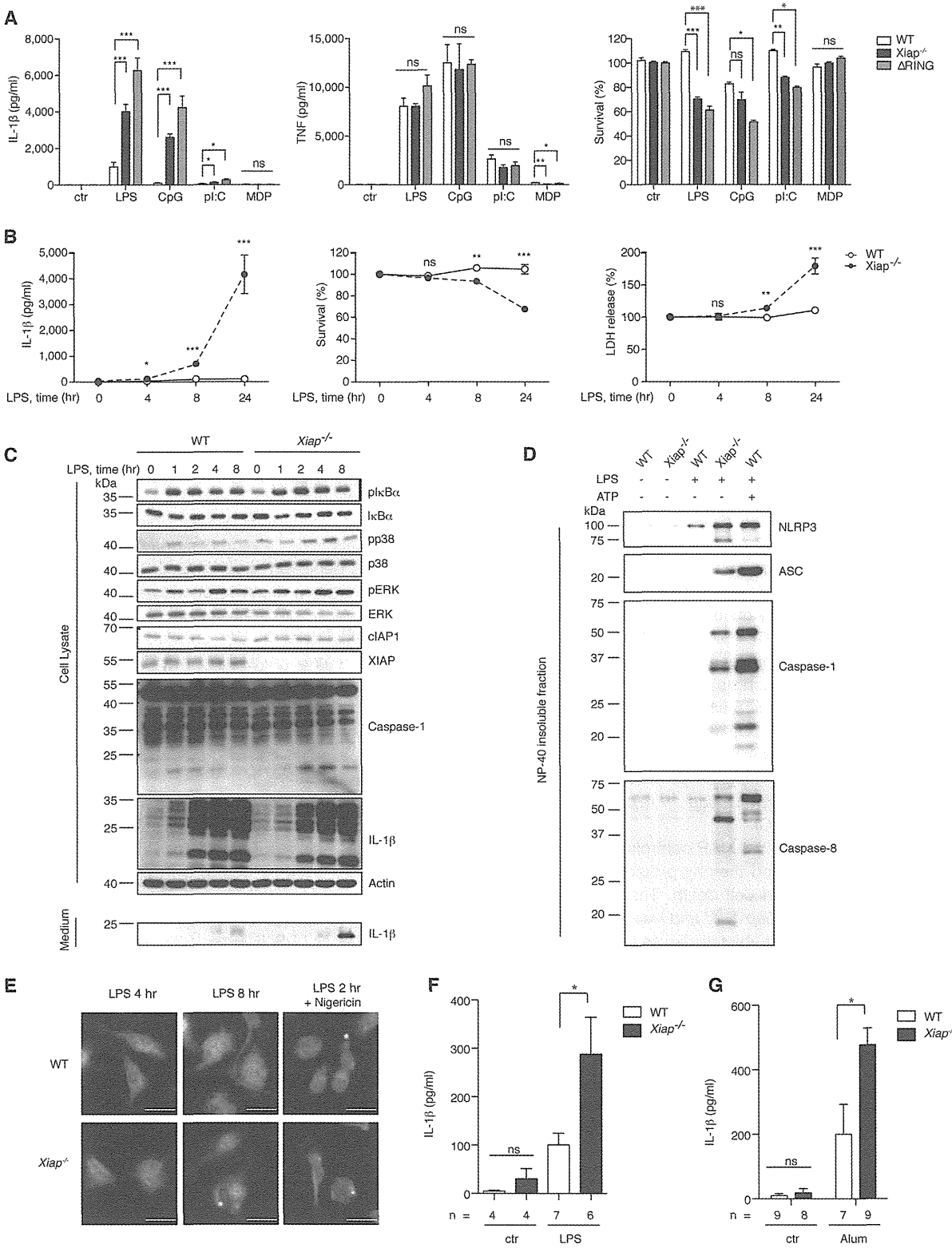

Figure 1. Exaggerated IL-1β Secretion in *Xiap*$^{-/-}$ and *Xiap*$^{\Delta RING}$ BMDCs and Mice

(A) Secreted IL-1β, TNF, and survival of WT, *Xiap*$^{-/-}$, and *Xiap*$^{\Delta RING}$ BMDCs treated with LPS, CpG (250 nM), polyI:C (10 μg/ml), or Muramyl dipeptide (MDP) (10 μg/ml) for 24 hr. ctr, control; ns, not significant.

(legend continued on next page)

transduction. Of note, we did not observe significant changes in NF-κB or MAPK signaling and gene induction in response to TNF in *Xiap*$^{-/-}$ and *Xiap*$^{\Delta RING}$ BMDCs (Figures S2C and S2D).

To better define the role of XIAP in the control of TNF signaling, we intercrossed *Xiap*$^{-/-}$ mice with mice deficient for TNF (*Tnf*^{tm1Gkl}) (Pasparakis et al., 1996). BMDCs from *Tnf*$^{-/-}$*Xiap*$^{-/-}$ double-deficient mice differentiated normally in culture (Figure S2E). Supporting a critical role of TNF/TNFR signaling for the observed phenotype, we found that genetic deletion of TNF reduced IL-1β secretion to WT levels after LPS (Figure 2B). Exogenous addition of recombinant TNF to *Tnf*$^{-/-}$*Xiap*$^{-/-}$ BMDCs fully recapitulated the excessive IL-1β production observed in *Xiap*$^{-/-}$ cells (Figure 2B). Deletion of TNF also rescued *Xiap*$^{-/-}$ BMDCs from cell death, implicating TNF-induced signaling events in both inflammasome activation and cell death (Figure 2B). Importantly, canonical inflammasome activation with ATP after a short priming stimulus with LPS caused normal inflammasome activation in *Tnf*$^{-/-}$ and *Tnf*$^{-/-}$*Xiap*$^{-/-}$ BMDCs (Figure S2F). This is in agreement with a previous report that showed that TNFR signaling was not required for canonical IL-1β maturation in response to a priming and activating signal when all IAPs were antagonized (Vince et al., 2012).

To understand the contribution of XIAP to IL-1β secretion and lymphoproliferation in vivo, we analyzed mice immunized with antigen-coated alum after 12 days. Alum induces a sustained inflammatory response primarily driven by NLRP3 inflammasome activation in inflammatory CD11c^{+} DCs (Eisenbarth et al., 2008; Kool et al., 2008). We observed an elevated splenic infiltration of inflammatory cells, such as neutrophils, macrophages, and eosinophils, in *Xiap*$^{-/-}$ mice when compared to WT mice (Jordan et al., 2004) (Figure 2C), which is reminiscent of the splenomegaly observed in many patients with XLP-2. In support of a critical role for TNF/TNFR signaling, we observed that the exaggerated splenic infiltration in *Xiap*$^{-/-}$ mice was absent in *Tnf*$^{-/-}$*Xiap*$^{-/-}$ mice (Figure 2C).

These data demonstrated that XIAP controls signaling events downstream of TNF/TNFR and thereby protects from aberrant inflammasome formation and cell death. The largely identical phenotype observed in both *Xiap*$^{\Delta RING}$ and *Xiap*$^{-/-}$ BMDCs implicated that XIAP functions as a ubiquitin ligase in this context.

Protection from Excessive Inflammasome Activation and Cell Death Is Predominantly Mediated by XIAP

Cell death triggered by TNF is often a consequence of deregulated ubiquitylation of RIP1 (Vandenabeele et al., 2010). cIAP1/cIAP2 are ubiquitin ligases of RIP1 and have been shown to protect from aberrant IL-1β secretion after TLR4 activation (Vince et al., 2012). To delineate the roles of cIAP1/cIAP2, from those of XIAP, we utilized the small molecule monovalent IAP antagonist (SMAC mimetic) LCL161. This compound has a higher affinity for cIAP1/cIAP2 than for XIAP and causes rapid degradation only of cIAP1/cIAP2, but not of XIAP (Figure 2D) (Weisberg et al., 2010).

cIAP1/cIAP2 depletion by LCL161 at 50 nM readily induced IL-1β secretion and cell death only in *Xiap*$^{-/-}$ cells, but not in WT cells (Figure 2E). Upon stimulation with LPS, WT cells depleted of cIAP1/cIAP2 failed to increase IL-1β secretion up to doses of 500 nM LCL161 (Figure 2F). In contrast, depletion of cIAP1/cIAP2 potently increased IL-1β secretion in *Xiap*$^{-/-}$ cells (Figure 2F). Interestingly, the IL-1β production was mostly TNF/TNFR dependent because *Tnf*$^{-/-}$ and *Tnf*$^{-/-}$*Xiap*$^{-/-}$ cells secreted significantly less IL-1β compared to WT and *Xiap*$^{-/-}$ cells, respectively (Figure 2F). A TNF-independent contribution to IL-1β secretion and cell death was observed only at LCL161 doses higher than 50 nM (Figure 2F).

To exclude the possibility that depletion of cIAP1 by LCL161 in *Xiap*$^{-/-}$ cells was not sufficient to deplete cIAP2 (Varfolomeev et al., 2007), we probed for NF-κB-inducing kinase (NIK) stabilization. We observed a similar elevation of NIK in both WT and *Xiap*$^{-/-}$ cells (Figures S2G and S2H), indicating that activation of the noncanonical NF-κB pathway did not contribute to the differential levels of IL-1β secretion and cell death.

In summary, depletion of cIAP1/cIAP2 was insufficient for IL-1β secretion and cell death to occur when XIAP was present. Depletion of cIAP1/cIAP2 only further promoted both outcomes when XIAP was deleted. We conclude that protection from excessive inflammasome activation and cell death in DCs after TNFR or TLR4 activation is predominantly mediated by XIAP.

RIP3 Is Required for Cell Death and Inflammasome Activation in *Xiap*$^{-/-}$ BMDCs after TNF/TNFR or TLR4 Stimulation

RIP3 is a mediator of TNF-induced cell death and inflammation (Murphy and Silke, 2014; Vandenabeele et al., 2010). We therefore determined the requirement for RIP3 for both outcomes in XIAP-deficient cells by crossing *Xiap*$^{-/-}$ mice with *Rip3*$^{-/-}$ mice (Newton et al., 2004). *Rip3*$^{-/-}$*Xiap*$^{-/-}$ BMDCs differentiated normally in culture (Figure S3A). After stimulation with TNF (Figure 3A) or LPS (Figures S3B and S3C), the secretion of processed IL-1β into the medium observed in *Xiap*$^{-/-}$ cells was completely abolished by loss of RIP3. The reduction in IL-1β levels correlated with normal cell survival in response to TNF or LPS, implying that inflammasome formation and cell death signaling are both consequences of RIP3 activity (Figures 3A and S3C). Surprisingly, processing of caspase-8 into the p17 subunit was absent in *Rip3*$^{-/-}$*Xiap*$^{-/-}$ BMDCs after TNF or LPS treatment (Figures 3B and S3B). In addition, deletion of

(B) Secreted IL-1β, cell viability, and LDH release of WT and *Xiap*$^{-/-}$ BMDCs treated with LPS (5 ng/ml).
(C) Immunoblotting of cell lysates and culture media from WT and *Xiap*$^{-/-}$ BMDCs treated with LPS (5 ng/ml).
(D) Immunoblotting of NP-40 insoluble fractions isolated from BMDCs after treatment with LPS (5 ng/ml) for 8 hr, or treatment with LPS for 2 hr plus ATP (5 mM) for 1 hr.
(E) Fluorescence microscopy of ASC/caspase-1 specks in WT and *Xiap*$^{-/-}$ BMDCs treated as indicated. Cells were stained for caspase-1 (yellow), nuclei (blue), and vimentin (red). Scale bars represent 20 μm.
(F and G) IL-1β from peritoneal fluid of WT and *Xiap*$^{-/-}$ mice injected with (F) LPS (1 μg) or (G) alum crystals (700 μg) i.p. for 2 hr. n, number of mice.
Error bars represent mean ± SEM. Other data represent mean ± SEM of at least three independent experiments performed in triplicates. See also Figure S1.

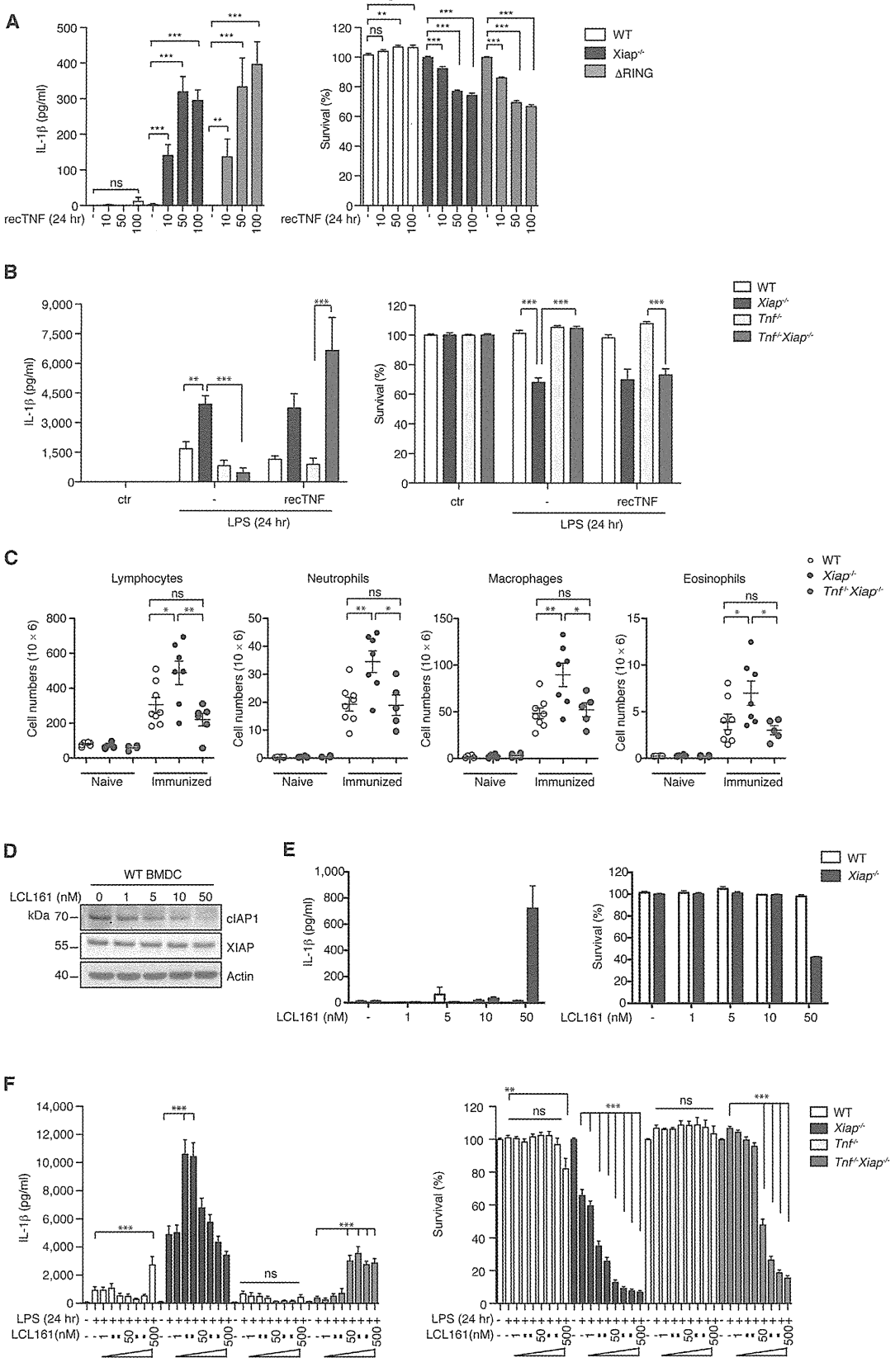

(legend on next page)

Rip3 blocked inflammasome formation as measured by assembly of ASC and caspase-1 within the NP-40 fraction (Figure 3C). The critical role of RIP3 was also confirmed in vivo, where the amount of IL-1β induced by LPS in *Xiap*$^{-/-}$ mice was reduced in *Rip3*$^{-/-}$*Xiap*$^{-/-}$ mice (Figure 3D). These findings identify XIAP as a negative regulator of RIP3-dependent signaling in response to TNF or LPS and detect a critical role for RIP3 in the full activation of caspase-8 in this process.

XIAP Regulates Ubiquitylation of RIP1 outside the TNF-RSC

The finding that XIAP restricted inflammasome activation and cell death downstream of TNF/TNFR signaling prompted us to investigate the impact of XIAP loss on the formation of the TNF-RSC. We performed immunoprecipitations of the TNF-RSC using FLAG-tagged TNF in WT or *Xiap*$^{-/y}$ HCT116 human colorectal carcinoma cells, which have previously been shown to fully form the TNF-RSC and propagate XIAP-dependent signaling (Damgaard et al., 2012; Krieg et al., 2009). We observed no differences in the composition or the ubiquitylation of proteins within the TNF-RSC when XIAP was absent (Figure S3D). This is in line with our data that showed no significant changes in NF-κB and MAPK activation, and gene induction, in *Xiap*$^{-/-}$ and *Xiap*$^{\Delta RING}$ BMDCs after TNF treatment (Figures S2C and S2D).

We next tested whether XIAP alters RIP1 expression by probing for the mRNA and protein levels of RIP1 in BMDCs. No significant changes were observed for RIP1 mRNA in response to either LPS or TNF (Figure S3E). However, compared to WT BMDCs, we observed elevated RIP1 protein levels in *Xiap*$^{-/-}$ cells at baseline and after 8 hr of LPS treatment (Figure 3E). The baseline elevation of RIP1 and the levels after stimulation were dependent on TNF signaling because RIP1 levels were lower in *Tnf*$^{-/-}$*Xiap*$^{-/-}$ cells (Figure 3E). The differences in protein levels despite normal mRNA expression suggest that XIAP affects RIP1 in a posttranslational manner.

We therefore examined whether changes in the ubiquitylation of RIP1 account for its increase. To pull down polyubiquitin chains from BMDCs, we utilized tandem ubiquitin binding entities (TUBEs) fused to glutathione S-transferase (GST). Intriguingly, we found that RIP1 ubiquitylation was substantially elevated after 30 and 60 min of TNF treatment in *Xiap*$^{-/-}$ BMDCs (Figure 3F). This finding was surprising because our data did not show an increase of ubiquitin on RIP1 within the TNF-RSC (Figure S3D) and because depletion of cIAP1/cIAP2 by SMAC mimetics reduces RIP1 ubiquitylation (Bertrand et al., 2008). These data therefore suggest that XIAP regulates RIP1 ubiquitylation independently from cIAP1/cIAP2 and outside the TNF-RSC.

We next investigated whether RIP3 contributes to the ubiquitylation of RIP1, possibly in a RIP1-RIP3-containing protein complex (Cho et al., 2009; Feoktistova et al., 2011; Tenev et al., 2011). We found that genetic deletion of RIP3 completely blocked the aberrant RIP1 ubiquitylation observed in *Xiap*$^{-/-}$ cells (Figure 3G). Collectively, these data show that XIAP contributes to the regulation of the ubiquitylation status of RIP1 in a RIP1-RIP3-containing complex outside of the TNF-RSC I.

Cell Death Is Induced Independently of Inflammasome Activation in *Xiap*$^{-/-}$ BMDCs

The critical role of RIP3 for the inflammasome activation and cell death induction in *Xiap*$^{-/-}$ cells prompted us to examine the relationship between both outcomes. We therefore generated *Caspase 1/11*$^{-/-}$*Xiap*$^{-/-}$ mice (Kuida et al., 1995). In line with previous literature, canonical inflammasome activation induced by ATP was completely blocked in BMDCs from such mice (Figures S4A and S4B).

After LPS treatment, we found a substantial reduction in IL-1β levels in *Caspase 1/11*$^{-/-}$*Xiap*$^{-/-}$ mice compared to *Xiap*$^{-/-}$ mice, implicating conventional inflammasome formation in this process (Figures 4A–4C). Interestingly, IL-1β levels in *Caspase 1/11*$^{-/-}$*Xiap*$^{-/-}$ mice at 24 hr were still substantially elevated compared to WT cells (Figure 4C). This suggested that processing of pro-IL-1β by caspase-8 might cooperate with caspase-1 for IL-1β maturation. Indeed, *Caspase 1/11*$^{-/-}$*Xiap*$^{-/-}$ BMDCs retained the elevated caspase-8 activity also observed in *Xiap*$^{-/-}$ cells (Figures 4A and 4B). Moreover, inhibition of caspase-8 with the inhibitor Z-IETD-FMK (IETD) further reduced IL-1β levels at 8 and 24 hr (Figures 4B and 4C), implying that caspase-8 contributes to IL-1β maturation in *Xiap*$^{-/-}$ BMDCs. We therefore tested the recruitment of both caspases into the NP-40 fraction in response to LPS. We observed that LPS treatment was sufficient to cause recruitment of caspase-8 and caspase-1 into this fraction in *Xiap*$^{-/-}$ cells, whereas WT cells required canonical inflammasome activation with ATP for this to occur (Figures 1D, 3C, and 4D). Of note, recruitment of caspase-8 to the NP-40 fraction was unperturbed in mice lacking caspase-1/caspase-11 (Figure 4D). In addition, inhibition of caspase-8 with IETD did not prevent caspase-1 recruitment to the NP-40 fraction in *Xiap*$^{-/-}$ cells (Figure 4E). Collectively, these data show that recruitment and activation of caspase-1 and caspase-8 occur independently of each other but that both cooperate in the processing of pro-IL-1β.

Importantly, we observed no effect of deletion of caspase-1/caspase-11 on the cell death of *Xiap*$^{-/-}$ cells (Figures 4B and 4C). Additional inhibition of caspase-8 (Figures 4B and 4C) and complete inhibition of all caspase activity using the caspase

Figure 2. XIAP Protects against Excessive IL-1β Secretion and Cell Death in a TNF-Dependent Manner

(A) IL-1β and cell survival of WT, *Xiap*$^{-/-}$, and *Xiap*$^{\Delta RING}$ BMDCs treated with recombinant TNF (recTNF) at 10, 50, and 100 ng/ml.

(B) IL-1β and cell viability of WT, *Xiap*$^{-/-}$, *Tnf*$^{-/-}$, and *Tnf*$^{-/-}$*Xiap*$^{-/-}$ BMDCs after LPS (5 ng/ml) with or without recTNF (100 ng/ml).

(C) Splenic lymphocytes, neutrophils, macrophages, and eosinophils from WT (n = 8), *Xiap*$^{-/-}$ (n = 7), and *Tnf*$^{-/-}$*Xiap*$^{-/-}$ (n = 5) mice 12 days after injection i.p. with coated alum crystals. Each dot represents a mouse, and error bars represent mean ± SEM.

(D) Immunoblots of WT BMDCs treated with IAP antagonist LCL161 for 2 hr.

(E) IL-1β and cell survival of WT and *Xiap*$^{-/-}$ BMDCs after LCL161 for 24 hr.

(F) IL-1β and cell viability of WT, *Xiap*$^{-/-}$, *Tnf*$^{-/-}$, and *Tnf*$^{-/-}$*Xiap*$^{-/-}$ BMDCs after LPS and LCL161 at 1, 5, 10, 50, 100, 200, and 500 nM for 24 hr.

Error bars represent mean ± SEM of at least three independent experiments performed in triplicates. See also Figure S2.

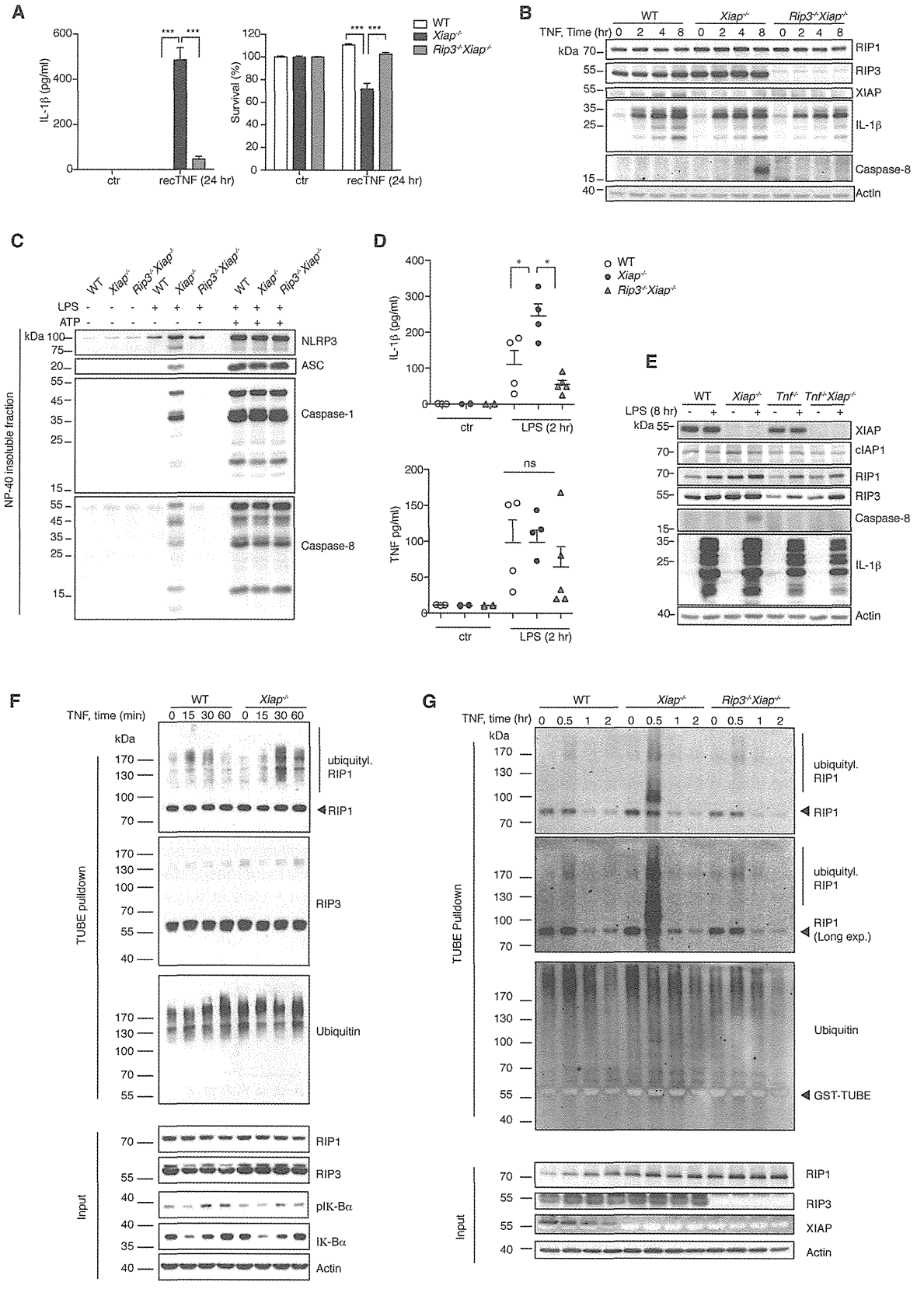

(legend on next page)

inhibitor ZVAD also failed to rescue the viability of *Xiap*$^{-/-}$ cells (Figure S4C). Whereas the precise function of caspase-8 in this context remains unresolved, our data clearly showed that cell death induction was nonapoptotic and independent from inflammasome activation.

Loss of XIAP Drives Excessive Inflammation in a Murine Model of EBV Mononucleosis

XLP-2 pathology in patients is often triggered by an Epstein-Barr virus (EBV) infection. As a murine model for EBV mononucleosis, we studied the immune response of *Xiap*$^{-/-}$ mice to murine γ-herpesvirus 68 (MHV-68) (Barton et al., 2011). In this model, intranasal (i.n.) infection with MHV-68 results in a productive infection of the respiratory tract (Stevenson and Efstathiou, 2005) that is followed by the transfer of the infection to lymphoid tissues. Latent infection is established in the spleen within 2–3 weeks postinfection (p.i.), after which the number of latently infected splenocytes returns to basal levels (Barton et al., 2011) (Figure 5A).

Despite normal viral clearance during early infection (days 6 and 16) (Figure 5B; data not shown), we found increased viral genomic loads in the spleens of infected *Xiap*$^{-/-}$ mice during late (day 43) and very late (day 84) latency (Figure 5B). On day 16, the cellularity of *Xiap*$^{-/-}$ and *Xiap*$^{\Delta RING}$ spleens was increased compared to those of WT mice, which was reflected by the increased numbers of myeloid and lymphoid populations in the spleen (Figure 5C). Because CD4^{+} T lymphocytes are important for the regulation of the viral loads of MHV-68, we measured T cell populations during active infection and early latency (Figure 5D). Despite equivalent values on day 6 p.i., the levels of CD4^{+} effector T cells, regulatory T cells (Treg), and IFNγ^{+} T cells were substantially elevated in *Xiap*$^{-/-}$ and *Xiap*$^{\Delta RING}$ mice at day 16 p.i., a phenotype also observed in patients with XLP-2 (Figure 5D).

In line with our in vitro data, we found substantially elevated IL-1β levels in the peripheral blood of *Xiap*$^{-/-}$ mice at day 16 p.i., whereas TNF was comparable between both genotypes (Figure 5E). Together, this shows that γ-herpesvirus infection drives hyperinflammation in *Xiap*$^{-/-}$ mice, similar to what is seen in EBV-infected patients with XLP-2.

Based on our findings showing the TNF-dependent nature of the excessive IL-1β secretion in *Xiap*$^{-/-}$ BMDCs and mice, we hypothesized that deletion of TNF would ameliorate some of the phenotypes observed. Indeed, during early infection at day 6 p.i., *Tnf*$^{-/-}$*Xiap*$^{-/-}$ mice failed to induce IL-1β induction, whereas at day 16 p.i., stimuli other than TNF induced IL-1β production comparable to the levels observed in *Xiap*$^{-/-}$ mice (Figure 5E). Consistently, we observed a reduction in myeloid and lymphoid subpopulations infiltrating the spleen in *Tnf*$^{-/-}$*Xiap*$^{-/-}$ mice at day 16 p.i. (Figures 5F and 5G). Finally, in agreement with our previous data, deletion of RIP3 also reduced the cellular infiltrations observed in spleens of *Xiap*$^{-/-}$ mice after viral infection (Figure S5A), further supporting a role for RIP3-dependent cell death and inflammation observed in *Xiap*$^{-/-}$ mice.

In summary, the phenotype observed in *Xiap*$^{-/-}$ and *Xiap*$^{\Delta RING}$ mice mimicked XLP-2 pathology, which is characterized by the effort of the immune system to clear an infectious pathogen, such as EBV, causing severe hyperinflammation. Importantly, genetic deletion of TNF ameliorated the symptoms, supporting the causative nature of TNF in this process and indicating a potential therapeutic benefit of TNF inhibition for patients with XLP-2 during early infection.

DISCUSSION

Excessive RIP3-dependent cell death has been shown to cause elevated cytokine production and inflammation collectively resulting in severe tissue damage (Murphy and Silke, 2014). This is exemplified, for example, by the development of severe terminal ileitis in Crohn's disease due to necroptosis of Paneth cells (Günther et al., 2011). Necroptosis-inhibiting proteins are therefore critical regulators of tissue homeostasis (Günther et al., 2011; Kang et al., 2013; Welz et al., 2011). Our data identify XIAP as an inhibitor of RIP3-dependent cell death and inflammation and show that loss of XIAP expression in mice causes hyperinflammation that mimics human XLP-2 pathology (Marsh et al., 2010).

Unexpectedly, our data place XIAP downstream of TNF signaling, despite the fact that it is not directly involved in the formation of the TNF-RSC I. The role of XIAP in TNFR signaling has mainly been characterized in mouse embryonic fibroblasts (MEFs). Contrary to cIAP1, XIAP is not involved in propagating canonical NF-κB activation in response to TNF in MEFs (Moulin et al., 2012) and fails to increase retention of RIP1 within the TNF signaling complex I (Vince et al., 2007). In contrast, our data place XIAP's function outside of the TNF-RSC I, where it controls the cellular fate of DCs by regulating RIP1 ubiquitylation together with RIP3 within a TNF/TNFR-induced signaling complex IIb (also termed ripoptosome or necrosome) (Murphy and Silke, 2014; Tenev et al., 2011). Whether XIAP directly interacts with RIP1 and/or RIP3 or whether the aberrant ubiquitylation of

Figure 3. TNF Induces Elevated Ubiquitylation of RIP1 and Drives RIP3-Dependent Inflammasome Formation and Cell Death in *Xiap*$^{-/-}$ Mice

(A) IL-1β secretion and survival of WT, *Xiap*$^{-/-}$, and *Rip3*$^{-/-}$*Xiap*$^{-/-}$ BMDCs treated with TNF (100 ng/ml). Data represent mean ± SEM of at least three independent experiments performed in triplicates.

(B) Immunoblots of WT, *Xiap*$^{-/-}$, and *Rip3*$^{-/-}$*Xiap*$^{-/-}$ BMDCs treated with TNF (100 ng/ml).

(C) Immunoblots of NP-40 insoluble fractions of WT, *Xiap*$^{-/-}$, and *Rip3*$^{-/-}$*Xiap*$^{-/-}$ BMDCs after LPS (5 ng/ml) for 8 hr, or LPS (10 ng/ml) primed for 2 hr plus ATP (5 mM) for 1 hr.

(D) Cytokines from peritoneal fluid of WT (n = 4), *Xiap*$^{-/-}$ (n = 4), and *Rip3*$^{-/-}$*Xiap*$^{-/-}$ (n = 5) mice after 2 hr of LPS (1 μg) i.p. Each data point represents one mouse. Error bars represent mean ± SEM.

(E) Immunoblots of extracts from WT, *Xiap*$^{-/-}$, *Tnf*$^{-/-}$, and *Tnf*$^{-/-}$*Xiap*$^{-/-}$ BMDCs after treatment with LPS (5 ng/ml).

(F) Immunoblots of GST-TUBE ubiquitin pull-down from WT and *Xiap*$^{-/-}$ BMDCs treated with TNF (100 ng/ml).

(G) Immunoblots of GST-TUBE ubiquitin pull-down from WT, *Xiap*$^{-/-}$, and *Rip3*$^{-/-}$ *Xiap*$^{-/-}$ BMDCs treated with TNF (100 ng/ml).

See also Figure S3.

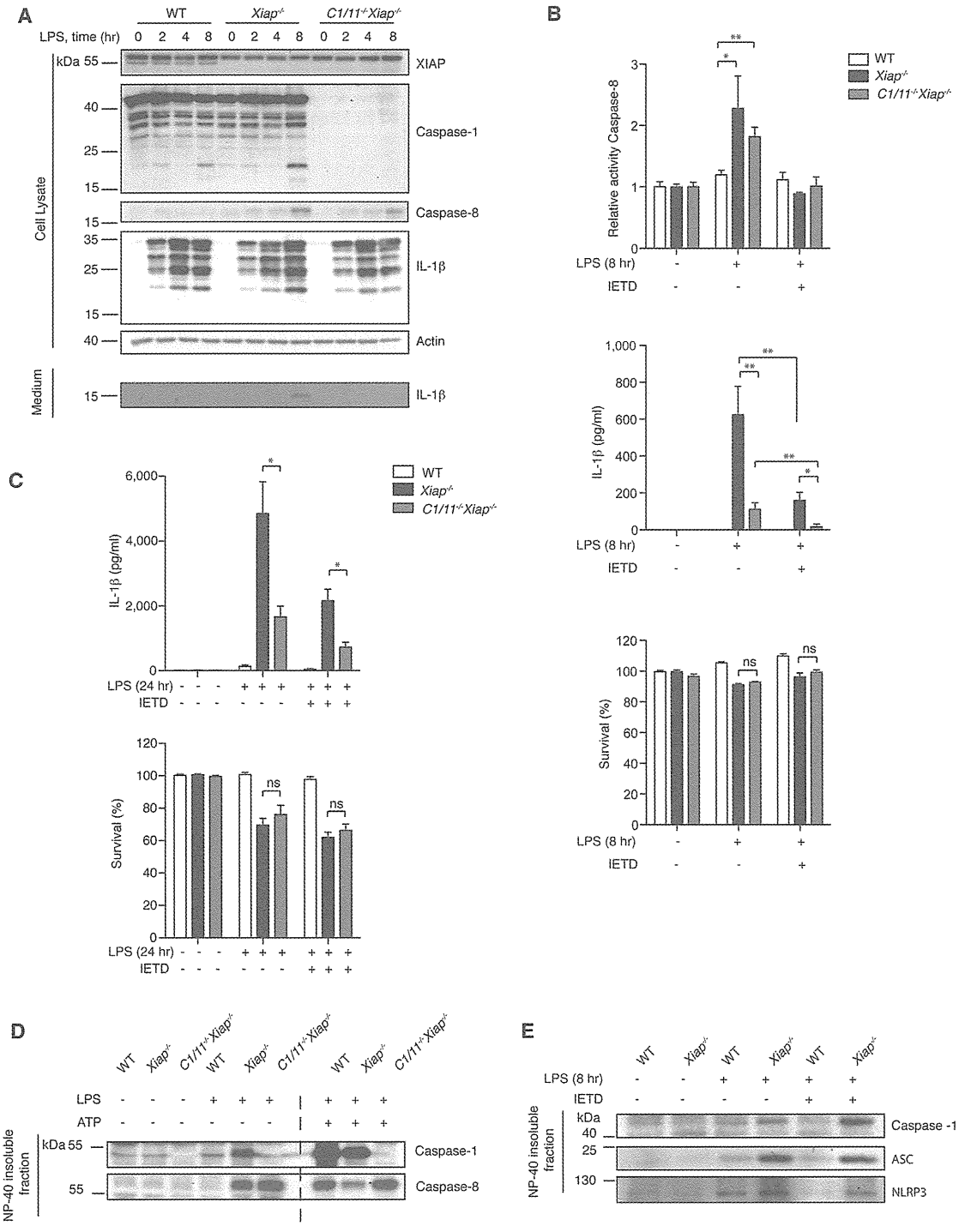

Figure 4. Caspase-1/Caspase-11 and Partially Caspase-8 Drive IL-1β Processing in *Xiap*$^{-/-}$ Mice, but Both Are Dispensable for Cell Death

(A) Immunoblots of cell extracts and media from WT, *Xiap*$^{-/-}$, and *Caspase 1/11*$^{-/-}$*Xiap*$^{-/-}$ BMDCs treated with LPS (5 ng/ml).

(B and C) Relative caspase-8 activity, IL-1β secretion, and survival of WT, *Xiap*$^{-/-}$, and *Caspase 1/11*$^{-/-}$*Xiap*$^{-/-}$ BMDCs after LPS (5 ng/ml) with or without the caspase-8 inhibitor IETD-fmk (IETD) (10 μM) for (B) 8 hr or (C) 24 hr.

(D) NP-40 insoluble fractions of WT, *Xiap*$^{-/-}$, and *Caspase 1/11*$^{-/-}$*Xiap*$^{-/-}$ BMDCs after LPS (5 ng/ml) for 8 hr, or LPS for 2 hr (10 ng/ml) plus ATP (5 mM) for 1 hr.

(E) NP-40 fractions of WT and *Xiap*$^{-/-}$ BMDCs with LPS (5 ng/ml) for 8 hr with or without IETD.

Error bars represent mean ± SEM of at least three independent experiments performed in triplicates. See also Figure S4.

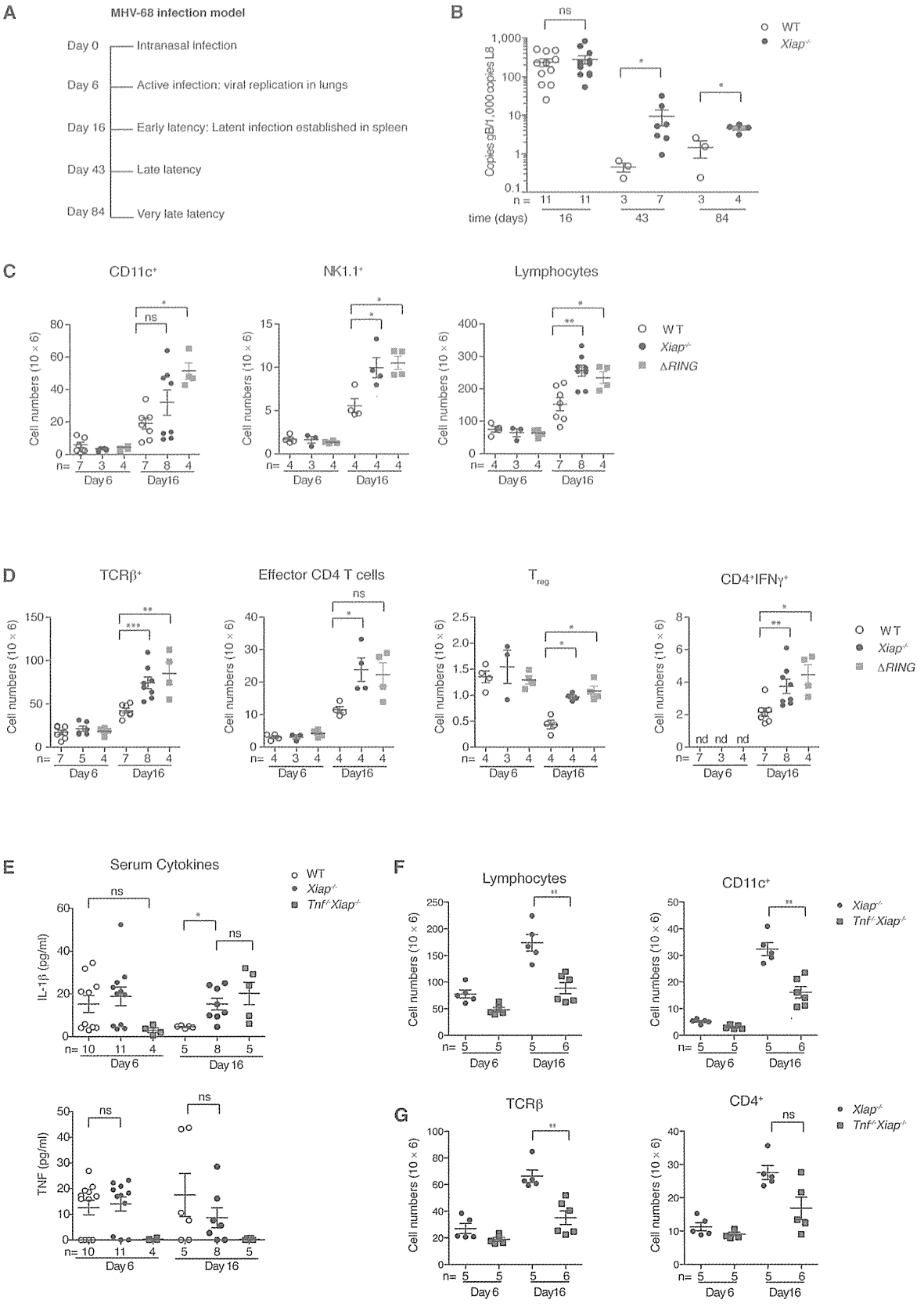

(legend on next page)

RIP1 favors binding to RIP3 remains unresolved, and these questions will be important to further investigate in the future.

The ubiquitylation status of RIP1 is a key factor that influences the switch between cell survival, apoptosis and RIP3-dependent cell death downstream of the TNFR. RIP1 has been shown to be decorated with M1, K11-, K48-, and K63-linked ubiquitin chains (Bertrand et al., 2011; Gerlach et al., 2011; Haas et al., 2009). cIAP1/cIAP2 have been implicated as mediators of the K48 and K63 linkages (Bertrand et al., 2011). Loss of these K48/K63 linkages, either via the action of specific deubiquitinases (DUBs) or by IAP antagonists, leads to cell death (Feoktistova et al., 2011; O'Donnell et al., 2011), whereas loss of the linear M1 linkage attenuates the NK-κB transcriptional response also resulting in elevated cell death (Gerlach et al., 2011; Haas et al., 2009; Ikeda et al., 2011). *Xiap*$^{\Delta RING}$ mutant mice, which express a truncated XIAP missing only the ligase function, presented with an almost identical phenotype compared to *Xiap*$^{-/-}$ mice. This supports the notion that XIAP functions as a ubiquitin ligase in TNFR/TNF signaling and that coordinated ubiquitylation events downstream of TNFR are tightly controlled by IAPs, including XIAP.

We observed an aberrant and prolonged ubiquitylation of RIP1 after TNF stimulation in cells lacking XIAP. Our data argue that XIAP functions as a ubiquitin ligase controlling the ubiquitylation of RIP1 either directly or indirectly, e.g., by affecting another ubiquitin ligase or DUB, which is important for ensuring correct RIP1 ubiquitylation. Indeed, there is emerging evidence that RIP1 ubiquitylation is tightly balanced by multiple ubiquitin ligases and DUBs and that altering this balance results in aberrant signaling and cell death (Gerlach et al., 2011; Keusekotten et al., 2013; O'Donnell et al., 2011; Wertz et al., 2004).

We show that XIAP cooperates with cIAP1/cIAP2 in diverging TNFR/TNF signaling away from cell death. However, XIAP clearly functions independently of cIAP1/cIAP2. This is exemplified by the fact that deletion of XIAP alone is sufficient to drive the observed phenotype and by the observation that deletion of XIAP causes aberrantly elevated ubiquitylation of RIP1 instead of the reduced RIP1 ubiquitylation observed when cIAP1/cIAP2 are inhibited (Bertrand et al., 2008)

XLP-2 is currently considered a familial hemophagocytic lymphohistiocytosis (HLH) disease despite the lack of the characteristic defects of CD8$^+$ T cell and natural killer cell cytotoxicity usually present in familial patients with HLH (Marsh et al., 2010). The protection of DCs and macrophages against RIP3-dependent cell death and inflammation afforded by XIAP argues that loss-of-function mutations constitute a major underlying cause of XLP-2 pathology. TNF was identified as the prime causative cytokine in our study, and genetic inhibition ameliorated some disease-specific symptoms. Despite the likely contribution of alternative inflammatory pathways, such as IFN signaling, we suggest that patients with XLP-2 might profit from therapeutic TNF inhibition when used early during an inflammatory episode (Mischler et al., 2007).

EXPERIMENTAL PROCEDURES

Mice

Xiap$^{-/-}$ (Olayioye et al., 2005) and *Xiap*$^{\Delta RING}$ (Schile et al., 2008) mice have been previously described. *Tnf tm1Gkl* (*Tnf*$^{-/-}$) (Pasparakis et al., 1996) and *Casp1*^{tm1Flv}*/J* (*Caspase-1/Caspase-11*$^{-/-}$) (Kuida et al., 1995) mice were purchased from Jackson Laboratories. *Rip3*$^{-/-}$ mice were obtained under a material transfer agreement from Genentech and have been previously described by Newton et al. (2004). Both male and female mice deficient for *BIRC4* were denoted *Xiap*$^{-/-}$. All animal experiments were performed in compliance with protocols approved by the local animal ethics committee guidelines.

Inflammasome Formation in BMDCs

To monitor inflammasome formation by fluorescence microscopy, cells treated with or without nigericin (5 μM) (Sigma-Aldrich) for 20–30 min after LPS priming for 2 hr were seeded on chamber slides and probed with antibodies against caspase-1 (Casper-2 clone; Adipogen) and vimentin (D21H3; Cell Signaling Technology). Images were acquired with a Leica DMRBE fluorescence microscope. For inflammasome-enrichment studies, cells were treated with LPS or TNF for the indicated times, and the insoluble fraction of the NP-40-lysed cells was collected by centrifugation and analyzed by SDS-PAGE and immunoblotting for ASC, caspase-1 (Casper-1 clone), as previously described (Gross et al., 2012).

Alum-Induced Peritonitis and Immunization

Eight to 12-week-old age- and sex-matched mice were injected i.p. with 700 μg Imject Alum Adjuvant (Thermo Scientific) in 200 μl PBS. Peritoneal fluid was collected 2 hr postinjection and concentrated to 100 μl with 10 kDa MWCO Vivaspin filters (Vivascience), and cytokines were measured by Cytokine Bead Array (BD Biosciences). For immunization, ovalbumin (100 μg) (Sigma-Aldrich; A2512) and LPS (10 μg) (Sigma-Aldrich; L2880) were precipitated with alum (4.4 μg) (Roth P724.1). Each mouse was injected with the precipitate that was washed once with PBS. Spleens of mice were analyzed by flow cytometry 12 days later.

Intranasal MHV-68 Infection

Intranasal (i.n) infection of mice was performed as previously described by El-Gogo et al. (2007) and Stevenson and Efstathiou (2005). In brief, mice were infected i.n. with 5×10^4 plaque-forming units. Lytic virus titers of infected lungs were determined on day 6, and splenic latent viral load was performed by real-time PCR. At days 6 and 16 p.i., spleens of infected mice were analyzed by flow cytometry analysis, and cytokines were measured from blood sera.

Statistical Analyses

The Wilcoxon-Mann-Whitney test was used to compare levels of serum cytokines and differences in cellular populations. All values are expressed as the mean ± SEM, and $p < 0.05$ (*), $p < 0.005$ (**), and $p < 0.0005$ (***) were

Figure 5. *Xiap*$^{-/-}$ and *Xiap*$^{\Delta RING}$ Mice Infected with MHV-68 Develop Excessive Inflammation

(A) Schematic overview of the MHV-68 infection model.

(B) MHV-68 viral genomic load of spleens from infected WT and *Xiap*$^{-/-}$ mice determined on days 16, 43, and 84 p.i.

(C) Flow cytometric analyses of spleens of infected WT, *Xiap*$^{-/-}$, and *Xiap*$^{\Delta RING}$ mice were analyzed at days 6 and 16 p.i.

(D) T cell subsets of infected mice were analyzed as in (C). Effector T cells were defined as TCRβ$^+$, CD4$^+$, CD44^{high}, CD62L^{low}, and T-regs as CD4$^+$, CD25$^+$, and FOXP3$^+$.

(E) IL-1β and TNF from sera of infected WT, *Xiap*$^{-/-}$, and *Tnf*$^{-/-}$*Xiap*$^{-/-}$ mice at days 6 and 16 p.i.

(F) Flow cytometric analysis of spleens of infected *Xiap*$^{-/-}$ and *Tnf*$^{-/-}$*Xiap*$^{-/-}$ mice at days 6 and 16 p.i.

(G) T cell numbers from mice in (F).

Each dot represents a mouse, and error bars represent mean ± SEM. See also Figure S5.

considered statistically significant. Statistical analyses and graphing were performed with GraphPad Prism software.

SUPPLEMENTAL INFORMATION

Supplemental Information includes Supplemental Experimental Procedures and five figures and can be found with this article online at http://dx.doi.org/10.1016/j.celrep.2014.05.008.

AUTHOR CONTRIBUTIONS

P.J.J. conceived and supervised the project, analyzed the data, and wrote the manuscript. M.Y. conceived and performed the experiments, analyzed the data, and wrote the manuscript. N.M., H.A., N.K., C.J.G., R.B.D., and O.G. performed experiments. H.K., M.R., and M.G.-H. provided critical reagents and samples. T.K., M.H., A.S., J.R., O.G., C.P., and M.G.-H. gave conceptual advice and wrote the paper.

ACKNOWLEDGMENTS

We thank H. Steller, C. Borner, D. Vaux, D. Porter, B. Vogelstein, L. O'Reilly, and Genentech and Novartis for gifts of mice and reagents; S. Rott, H. Bendz, J. Christian, D. Kull, R. Hillermann, B. Steer, and M. Strehle for excellent technical assistance; and R. Holmes (Berlin) for language support. P.J.J. was supported by a Max Eder-Program grant from the Deutsche Krebshilfe (program #109310), a Human Frontiers Science Program grant (program #RGY0073/2012), and the German Jose Carreras Leukemia Foundation grant (DJCLS R 12/22). H.A. was supported by grants from Wilhelm Sander-Stiftung (2009.046.1+2) and the BMBF (NGFNplus, PIM-01GS0802-3). M.H. was supported by the Helmholtz-Foundation and the Peter-Hans Hofschneider Foundation. N.M. and C.J.G. are members of the TUM Graduate School. C.J.G. is supported by the Natural Science and Engineering Research Council of Canada. O.G. is supported by the Bavarian Molecular Biosystems Research Network. M.G.-H. is supported by a Steno Fellowship from the Danish Council for Independent Research-Natural Sciences, the Lundbeck Foundation, and the Novo Nordisk Foundation.

Received: September 24, 2013
Revised: April 10, 2014
Accepted: May 5, 2014
Published: May 29, 2014

REFERENCES

Barton, E., Mandal, P., and Speck, S.H. (2011). Pathogenesis and host control of gammaherpesviruses: lessons from the mouse. Annu. Rev. Immunol. *29*, 351–397.

Bauler, L.D., Duckett, C.S., and O'Riordan, M.X. (2008). XIAP regulates cytosol-specific innate immunity to Listeria infection. PLoS Pathog. *4*, e1000142.

Bertrand, M.J., Milutinovic, S., Dickson, K.M., Ho, W.C., Boudreault, A., Durkin, J., Gillard, J.W., Jaquith, J.B., Morris, S.J., and Barker, P.A. (2008). cIAP1 and cIAP2 facilitate cancer cell survival by functioning as E3 ligases that promote RIP1 ubiquitination. Mol. Cell *30*, 689–700.

Bertrand, M.J., Lippens, S., Staes, A., Gilbert, B., Roelandt, R., De Medts, J., Gevaert, K., Declercq, W., and Vandenabeele, P. (2011). cIAP1/2 are direct E3 ligases conjugating diverse types of ubiquitin chains to receptor interacting proteins kinases 1 to 4 (RIP1-4). PLoS One *6*, e22356.

Cho, Y.S., Challa, S., Moquin, D., Genga, R., Ray, T.D., Guildford, M., and Chan, F.K. (2009). Phosphorylation-driven assembly of the RIP1-RIP3 complex regulates programmed necrosis and virus-induced inflammation. Cell *137*, 1112–1123.

Damgaard, R.B., Nachbur, U., Yabal, M., Wong, W.W., Fiil, B.K., Kastirr, M., Rieser, E., Rickard, J.A., Bankovacki, A., Peschel, C., et al. (2012). The ubiquitin ligase XIAP recruits LUBAC for NOD2 signaling in inflammation and innate immunity. Mol. Cell *46*, 746–758.

Damgaard, R.B., Fiil, B.K., Speckmann, C., Yabal, M., zur Stadt, U., Bekker-Jensen, S., Jost, P.J., Ehl, S., Mailand, N., and Gyrd-Hansen, M. (2013). Disease-causing mutations in the XIAP BIR2 domain impair NOD2-dependent immune signalling. EMBO Mol. Med. *5*, 1278–1295.

Deveraux, Q.L., Takahashi, R., Salvesen, G.S., and Reed, J.C. (1997). X-linked IAP is a direct inhibitor of cell-death proteases. Nature *388*, 300–304.

Eisenbarth, S.C., Colegio, O.R., O'Connor, W., Sutterwala, F.S., and Flavell, R.A. (2008). Crucial role for the Nalp3 inflammasome in the immunostimulatory properties of aluminium adjuvants. Nature *453*, 1122–1126.

El-Gogo, S., Staib, C., Meyr, M., Erfle, V., Sutter, G., and Adler, H. (2007). Recombinant murine gammaherpesvirus 68 (MHV-68) as challenge virus to test efficacy of vaccination against chronic virus infections in the mouse model. Vaccine *25*, 3934–3945.

Feoktistova, M., Geserick, P., Kellert, B., Dimitrova, D.P., Langlais, C., Hupe, M., Cain, K., MacFarlane, M., Häcker, G., and Leverkus, M. (2011). cIAPs block Ripoptosome formation, a RIP1/caspase-8 containing intracellular cell death complex differentially regulated by cFLIP isoforms. Mol. Cell *43*, 449–463.

Gerlach, B., Cordier, S.M., Schmukle, A.C., Emmerich, C.H., Rieser, E., Haas, T.L., Webb, A.I., Rickard, J.A., Anderton, H., Wong, W.W., et al. (2011). Linear ubiquitination prevents inflammation and regulates immune signalling. Nature *471*, 591–596.

Gross, O., Yazdi, A.S., Thomas, C.J., Masin, M., Heinz, L.X., Guarda, G., Quadroni, M., Drexler, S.K., and Tschopp, J. (2012). Inflammasome activators induce interleukin-1α secretion via distinct pathways with differential requirement for the protease function of caspase-1. Immunity *36*, 388–400.

Günther, C., Martini, E., Wittkopf, N., Amann, K., Weigmann, B., Neumann, H., Waldner, M.J., Hedrick, S.M., Tenzer, S., Neurath, M.F., and Becker, C. (2011). Caspase-8 regulates TNF-α-induced epithelial necroptosis and terminal ileitis. Nature *477*, 335–339.

Gyrd-Hansen, M., and Meier, P. (2010). IAPs: from caspase inhibitors to modulators of NF-kappaB, inflammation and cancer. Nat. Rev. Cancer *10*, 561–574.

Haas, T.L., Emmerich, C.H., Gerlach, B., Schmukle, A.C., Cordier, S.M., Rieser, E., Feltham, R., Vince, J., Warnken, U., Wenger, T., et al. (2009). Recruitment of the linear ubiquitin chain assembly complex stabilizes the TNF-R1 signaling complex and is required for TNF-mediated gene induction. Mol. Cell *36*, 831–844.

Ikeda, F., Deribe, Y.L., Skånland, S.S., Stieglitz, B., Grabbe, C., Franz-Wachtel, M., van Wijk, S.J., Goswami, P., Nagy, V., Terzic, J., et al. (2011). SHARPIN forms a linear ubiquitin ligase complex regulating NF-κB activity and apoptosis. Nature *471*, 637–641.

Jordan, M.B., Mills, D.M., Kappler, J., Marrack, P., and Cambier, J.C. (2004). Promotion of B cell immune responses via an alum-induced myeloid cell population. Science *304*, 1808–1810.

Jost, P.J., Grabow, S., Gray, D., McKenzie, M.D., Nachbur, U., Huang, D.C., Bouillet, P., Thomas, H.E., Borner, C., Silke, J., et al. (2009). XIAP discriminates between type I and type II FAS-induced apoptosis. Nature *460*, 1035–1039.

Kang, T.B., Yang, S.H., Toth, B., Kovalenko, A., and Wallach, D. (2013). Caspase-8 blocks kinase RIPK3-mediated activation of the NLRP3 inflammasome. Immunity *38*, 27–40.

Keusekotten, K., Elliott, P.R., Glockner, L., Fiil, B.K., Damgaard, R.B., Kulathu, Y., Wauer, T., Hospenthal, M.K., Gyrd-Hansen, M., Krappmann, D., et al. (2013). OTULIN antagonizes LUBAC signaling by specifically hydrolyzing Met1-linked polyubiquitin. Cell *153*, 1312–1326.

Kool, M., Soullié, T., van Nimwegen, M., Willart, M.A., Muskens, F., Jung, S., Hoogsteden, H.C., Hammad, H., and Lambrecht, B.N. (2008). Alum adjuvant boosts adaptive immunity by inducing uric acid and activating inflammatory dendritic cells. J. Exp. Med. *205*, 869–882.

Krieg, A., Correa, R.G., Garrison, J.B., Le Negrate, G., Welsh, K., Huang, Z., Knoefel, W.T., and Reed, J.C. (2009). XIAP mediates NOD signaling via interaction with RIP2. Proc. Natl. Acad. Sci. USA *106*, 14524–14529.

Kuida, K., Lippke, J.A., Ku, G., Harding, M.W., Livingston, D.J., Su, M.S., and Flavell, R.A. (1995). Altered cytokine export and apoptosis in mice deficient in interleukin-1 beta converting enzyme. Science *267*, 2000–2003.

Lamkanfi, M., and Dixit, V.M. (2012). Inflammasomes and their roles in health and disease. Annu. Rev. Cell Dev. Biol. *28*, 137–161.

Marsh, R.A., Madden, L., Kitchen, B.J., Mody, R., McClimon, B., Jordan, M.B., Bleesing, J.J., Zhang, K., and Filipovich, A.H. (2010). XIAP deficiency: a unique primary immunodeficiency best classified as X-linked familial hemophagocytic lymphohistiocytosis and not as X-linked lymphoproliferative disease. Blood *116*, 1079–1082.

Martinon, F., Burns, K., and Tschopp, J. (2002). The inflammasome: a molecular platform triggering activation of inflammatory caspases and processing of proIL-beta. Mol. Cell *10*, 417–426.

Mischler, M., Fleming, G.M., Shanley, T.P., Madden, L., Levine, J., Castle, V., Filipovich, A.H., and Cornell, T.T. (2007). Epstein-Barr virus-induced hemophagocytic lymphohistiocytosis and X-linked lymphoproliferative disease: a mimicker of sepsis in the pediatric intensive care unit. Pediatrics *119*, e1212–e1218.

Moulin, M., Anderton, H., Voss, A.K., Thomas, T., Wong, W.W., Bankovacki, A., Feltham, R., Chau, D., Cook, W.D., Silke, J., and Vaux, D.L. (2012). IAPs limit activation of RIP kinases by TNF receptor 1 during development. EMBO J. *31*, 1679–1691.

Murphy, J.M., and Silke, J. (2014). Ars Moriendi; the art of dying well - new insights into the molecular pathways of necroptotic cell death. EMBO Rep. *15*, 155–164.

Murphy, J.M., Czabotar, P.E., Hildebrand, J.M., Lucet, I.S., Zhang, J.G., Alvarez-Diaz, S., Lewis, R., Lalaoui, N., Metcalf, D., Webb, A.I., et al. (2013). The pseudokinase MLKL mediates necroptosis via a molecular switch mechanism. Immunity *39*, 443–453.

Newton, K., Sun, X., and Dixit, V.M. (2004). Kinase RIP3 is dispensable for normal NF-kappa Bs, signaling by the B-cell and T-cell receptors, tumor necrosis factor receptor 1, and Toll-like receptors 2 and 4. Mol. Cell. Biol. *24*, 1464–1469.

O'Donnell, M.A., Perez-Jimenez, E., Oberst, A., Ng, A., Massoumi, R., Xavier, R., Green, D.R., and Ting, A.T. (2011). Caspase 8 inhibits programmed necrosis by processing CYLD. Nat. Cell Biol. *13*, 1437–1442.

Olayioye, M.A., Kaufmann, H., Pakusch, M., Vaux, D.L., Lindeman, G.J., and Visvader, J.E. (2005). XIAP-deficiency leads to delayed lobuloalveolar development in the mammary gland. Cell Death Differ. *12*, 87–90.

Pachlopnik Schmid, J., Canioni, D., Moshous, D., Touzot, F., Mahlaoui, N., Hauck, F., Kanegane, H., Lopez-Granados, E., Mejstrikova, E., Pellier, I., et al. (2011). Clinical similarities and differences of patients with X-linked lymphoproliferative syndrome type 1 (XLP-1/SAP deficiency) versus type 2 (XLP-2/XIAP deficiency). Blood *117*, 1522–1529.

Pasparakis, M., Alexopoulou, L., Episkopou, V., and Kollias, G. (1996). Immune and inflammatory responses in TNF alpha-deficient mice: a critical requirement for TNF alpha in the formation of primary B cell follicles, follicular dendritic cell networks and germinal centers, and in the maturation of the humoral immune response. J. Exp. Med. *184*, 1397–1411.

Prakash, H., Albrecht, M., Becker, D., Kuhlmann, T., and Rudel, T. (2010). Deficiency of XIAP leads to sensitization for Chlamydophila pneumoniae pulmonary infection and dysregulation of innate immune response in mice. J. Biol. Chem. *285*, 20291–20302.

Rigaud, S., Fondanèche, M.C., Lambert, N., Pasquier, B., Mateo, V., Soulas, P., Galicier, L., Le Deist, F., Rieux-Laucat, F., Revy, P., et al. (2006). XIAP deficiency in humans causes an X-linked lymphoproliferative syndrome. Nature *444*, 110–114.

Schile, A.J., García-Fernández, M., and Steller, H. (2008). Regulation of apoptosis by XIAP ubiquitin-ligase activity. Genes Dev. *22*, 2256–2266.

Stevenson, P.G., and Efstathiou, S. (2005). Immune mechanisms in murine gammaherpesvirus-68 infection. Viral Immunol. *18*, 445–456.

Tenev, T., Bianchi, K., Darding, M., Broemer, M., Langlais, C., Wallberg, F., Zachariou, A., Lopez, J., MacFarlane, M., Cain, K., and Meier, P. (2011). The Ripoptosome, a signaling platform that assembles in response to genotoxic stress and loss of IAPs. Mol. Cell *43*, 432–448.

Vandenabeele, P., Declercq, W., Van Herreweghe, F., and Vanden Berghe, T. (2010). The role of the kinases RIP1 and RIP3 in TNF-induced necrosis. Sci. Signal. *3*, re4.

Varfolomeev, E., Blankenship, J.W., Wayson, S.M., Fedorova, A.V., Kayagaki, N., Garg, P., Zobel, K., Dynek, J.N., Elliott, L.O., Wallweber, H.J., et al. (2007). IAP antagonists induce autoubiquitination of c-IAPs, NF-kappaB activation, and TNFalpha-dependent apoptosis. Cell *131*, 669–681.

Vince, J.E., Wong, W.W., Khan, N., Feltham, R., Chau, D., Ahmed, A.U., Benetatos, C.A., Chunduru, S.K., Condon, S.M., McKinlay, M., et al. (2007). IAP antagonists target cIAP1 to induce TNFalpha-dependent apoptosis. Cell *131*, 682–693.

Vince, J.E., Wong, W.W., Gentle, I., Lawlor, K.E., Allam, R., O'Reilly, L., Mason, K., Gross, O., Ma, S., Guarda, G., et al. (2012). Inhibitor of apoptosis proteins limit RIP3 kinase-dependent interleukin-1 activation. Immunity *36*, 215–227.

Wada, T., Kanegane, H., Ohta, K., Katoh, F., Imamura, T., Nakazawa, Y., Miyashita, R., Hara, J., Hamamoto, K., Yang, X., et al. (2014). Sustained elevation of serum interleukin-18 and its association with hemophagocytic lymphohistiocytosis in XIAP deficiency. Cytokine *65*, 74–78.

Weisberg, E., Ray, A., Barrett, R., Nelson, E., Christie, A.L., Porter, D., Straub, C., Zawel, L., Daley, J.F., Lazo-Kallanian, S., et al. (2010). Smac mimetics: implications for enhancement of targeted therapies in leukemia. Leukemia *24*, 2100–2109.

Welz, P.S., Wullaert, A., Vlantis, K., Kondylis, V., Fernández-Majada, V., Ermolaeva, M., Kirsch, P., Sterner-Kock, A., van Loo, G., and Pasparakis, M. (2011). FADD prevents RIP3-mediated epithelial cell necrosis and chronic intestinal inflammation. Nature *477*, 330–334.

Wertz, I.E., O'Rourke, K.M., Zhou, H., Eby, M., Aravind, L., Seshagiri, S., Wu, P., Wiesmann, C., Baker, R., Boone, D.L., et al. (2004). De-ubiquitination and ubiquitin ligase domains of A20 downregulate NF-kappaB signalling. Nature *430*, 694–699.